SCIENTIFIC REPORTS
nature research

OPEN

Multicoding in neural information transfer suggested by mathematical analysis of the frequency-dependent synaptic plasticity in vivo

Katsuhiko Hata[1,3,5]✉, Osamu Araki[2], Osamu Yokoi[3], Tatsumi Kusakabe[1], Yoshio Yamamoto[4], Susumu Ito[1] & Tetsuro Nikuni[5]

Two elements of neural information processing have primarily been proposed: firing rate and spike timing of neurons. In the case of synaptic plasticity, although spike-timing-dependent plasticity (STDP) depending on presynaptic and postsynaptic spike times had been considered the most common rule, recent studies have shown the inhibitory nature of the brain in vivo for precise spike timing, which is key to the STDP. Thus, the importance of the firing frequency in synaptic plasticity in vivo has been recognized again. However, little is understood about how the frequency-dependent synaptic plasticity (FDP) is regulated in vivo. Here, we focused on the presynaptic input pattern, the intracellular calcium decay time constants, and the background synaptic activity, which vary depending on neuron types and the anatomical and physiological environment in the brain. By analyzing a calcium-based model, we found that the synaptic weight differs depending on these factors characteristic in vivo, even if neurons receive the same input rate. This finding suggests the involvement of multifaceted factors other than input frequency in FDP and even neural coding in vivo.

Synaptic plasticity in neural networks is a substrate of learning and memory, which includes both positive and negative components, i.e., both long-lasting enhancements and declines in the weight of synaptic transmission (long-term potentiation (LTP) and long-term depression (LTD))[1]. Many experimental studies have suggested two plausible mechanisms for the induction of the synaptic plasticity[2,3]. The first is the frequency of spike trains, which has been studied in association with the Bienenstock, Cooper, and Munro (BCM) rule in classical research conducted approximately half a century ago[4–6]. LTP is induced by high-frequency firing in presynaptic neurons, which produces large increases in postsynaptic calcium concentration[5–8]. The low-frequency firing causes a modest increase in the calcium level, and thereby induces LTD[9–11]. The second is the precise timing of presynaptic and postsynaptic firing, which has been investigated as spike-time-dependent plasticity (STDP) in numerous experimental and theoretical studies from approximately 20 years ago[12–15]. LTP is induced by the presynaptic action potentials preceding postsynaptic spikes by no more than tens of milliseconds, whereas presynaptic firing that follows postsynaptic spikes produces LTD[13,14,16–19]. The idea that STDP plays a central role in synaptic plasticity had been becoming mainstream.

Recent studies have reported, however, that in some cases, the environment in vivo may not be suitable for precise spike timing, which is key to the STDP. Pre- and post-synaptic neurons in the primary visual cortex and extrastriate cortex of awaking animals fire so irregularly that the timing of presynaptic and postsynaptic firing varies[20–22]. Neurons and synapses in the cerebral cortex of rats receive a lot of background neuronal activity that is generated internally, which provides strong constraints on spike timing[23–25]. In these environments, the

[1]Department of Sports and Medical Science, Kokushikan University, Tokyo, Japan. [2]Department of Applied Physics, Faculty of Science Division I, Tokyo University of Science, Tokyo, Japan. [3]Department of Neuroscience, Research Center for Mathematical Medicine, Tokyo, Japan. [4]Laboratory of Veterinary Biochemistry and Cell Biology, Faculty of Agriculture, Iwate University, Morioka, Japan. [5]Department of Physics, Faculty of Science Division I, Tokyo University of Science, Tokyo, Japan. ✉email: khata@kokushikan.ac.jp

firing rate, rather than the spike timing, is likely to be important for the synaptic plasticity and neural coding. For example, it has been demonstrated experimentally that the cerebral cortex in which there is a high level of internal noise uses a rate code[25], and it has been shown mathematically that synaptic changes are induced by variation of firing rate without any timing constraints[20]. The firing rate may also be an essential factor for the STDP. Recently, Madadi Asl et al. revealed that STDP model incorporating dendritic and axonal propagation delay can adequately explain the existence of recurrent connections between pairs of neurons in the cerebral cortex[26]. They found that the firing frequency plays an essential role in the formation of connectivity patterns in Two-Neuron Motif[27]. Moreover, firing variability, as well as the statistical properties of the spike frequency, seems essential for real-time information processing[28].

Based on these reports, the role of firing frequency in various aspects of neural information processing has again come into the limelight. Furthermore, in vivo characteristic factors such as the variation of the firing pattern, the difference of intracellular parameters, and internal noise have also been suggested to be important for synaptic plasticity and neural coding[20,28–32]. However, how these factors are involved in the synaptic plasticity is poorly understood. In order to clarify this problem, we examined the role of the presynaptic input pattern, the intracellular calcium decay time constants, and the background synaptic activity in frequency-dependent synaptic plasticity (FDP) by analyzing a calcium-based model, which is one of the most compatible models with experimental results[12,33].

Currently, it is widely accepted that the calcium concentration in the postsynapse determines whether LTP or LTD is induced[34–37]. A moderate elevation of intracellular calcium correlates with induction of LTD, whereas a larger increase correlates with LTP[35,36]. Only if glutamate is released by presynaptic activity and if the postsynaptic membrane is depolarized sufficiently, calcium ions enter the cell through channels controlled by NMDA receptors[12]. The depolarization of the postsynaptic membrane potential is due not only to excitatory postsynaptic potentials (EPSPs) generated by binding glutamate to the AMPA receptors but also to many kinds of background synaptic activities[38–41]. These experimental events were formulated by Shouval et al.[33] as a calcium-based model (from now on, we call it "Shouval's model"), which has been used in numerous studies.

In the present study, we investigated the FDP in vivo analytically and numerically using the Shouval's model. First, to investigate the FDP in neurons with in vivo-specific firing pattern, we used three types of firing, which are widely observed in the brain, that is, constant-inter-spike intervals (ISI) inputs, Poisson inputs, and gamma inputs. Next, the calcium decay time constant of in vivo neurons varies from cell to cell. Previous reports suggested that pyramidal neurons in superficial layers possess faster calcium dynamics than those in deep layers. Here, $\tau_{ca} \approx 40$ ms in layer II to IV neurons, whereas $\tau_{ca} \approx 100$ ms in layer V to VI neurons[42,43]. To study the association of the calcium decay time constant with the FDP, we examined two kinds of neurons with time constants of 40 ms and 80 ms. Finally, neurons in vivo are constantly exposed to background synaptic activity[38,41]. The frequency and magnitude of this activity vary depending on the location of the synapse and the level of neuronal activity[38,41]. We, therefore, examined the correlation between the amplitude of background activity and the FDP. The findings in the present study may contribute to a detailed understanding of synaptic plasticity in in vivo brain.

Results

We used a model for the FDP based on the calcium control hypothesis of Shouval et al., assuming that the change of the synaptic weight is fully determined by the postsynaptic calcium level[33,44]. This model has been confirmed to integrate STDP observed in acute hippocampal slices within a single theoretical framework[45]. Among the few studies that have analytically solved this hypothesis, Yeung et al.[46] calculated the mean values of the calcium transients evoked by a spiking neuron. In the present study, we analytically derived the intracellular calcium concentration and synaptic weight with respect to the input frequency focusing only on the long-term behavior of the intracellular calcium concentration and synaptic weight.

Postsynaptic calcium concentration as a function of the presynaptic stimulation frequency with fixed interstimulus intervals. In order to investigate the dependence of the postsynaptic calcium concentration on the average presynaptic stimulation frequency of each input pattern, we first developed an analytical solution of the postsynaptic calcium concentration with constant-ISI inputs as a control. In Fig. 1, we plot the analytical solution of Ca in Eq. (42) as a function of the input frequency f. We also plot the simulation results obtained by solving Eqs. (9)–(18) numerically as a function of time and taking the time average of Ca for each frequency. The analytical solution for the long-term behavior of calcium level agrees very well with the numerical simulation results. We adopted $\tau_{Ca} = 80$ ms for a long calcium decay time constant and $\tau_{Ca} = 40$ ms as a short calcium decay time constant. The calcium concentration as a function of input frequency increases slower for $\tau_{Ca} = 40$ ms than for $\tau_{Ca} = 80$ ms. Equation (42) indicates that the calcium concentration at an arbitrary stimulation rate increases linearly for the calcium decay time constant τ_{Ca}.

Approximate analytic solution of synaptic weight as a function of the input frequency with fixed interstimulus intervals. Figure 2 shows the curve obtained by performing the integration in Eq. (51). We also plot the results obtained by the numerical simulation, which agree qualitatively with the analytical results. These results suggest that the LTD/LTP threshold shifts to a lower frequency as the calcium decay time constant increases. Here, the LTD/LTP threshold is defined as the frequency at which the synaptic weight first returns to 1 after falling below 1 when the input frequency is increased from 0 Hz. This tendency can also be understood from Eq. (42) as follows. Equation (42) is written as $Ca(f) = \tau_{Ca} \cdot F(f)$, where $F(f)$ is a monotonically increasing function of f, so that f can be formally expressed as

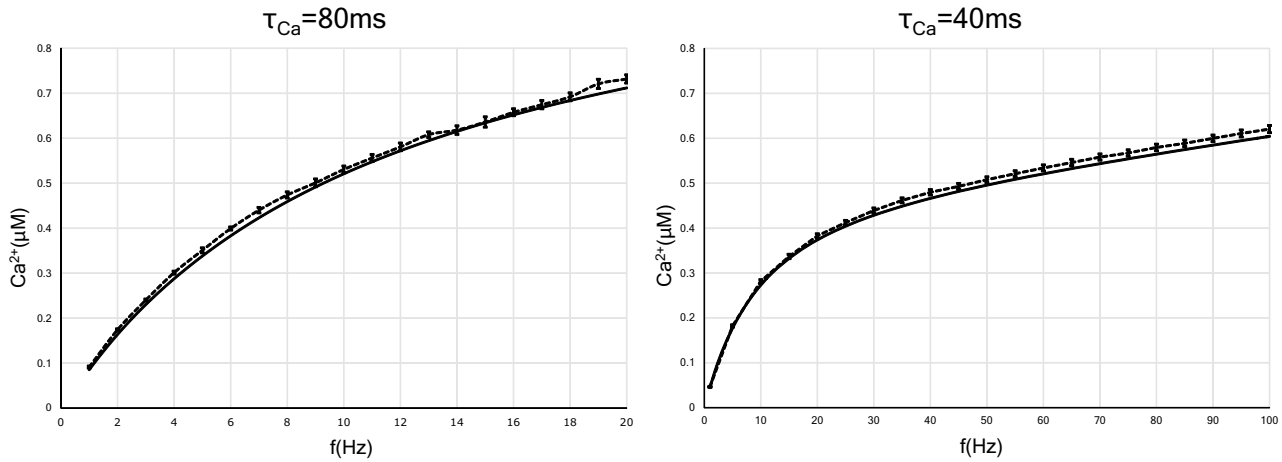

Figure 1. Presynaptic firing rate-induced elevation of intracellular calcium concentration in two types of neurons with different time constants of calcium decay. The analytic solution is indicated by solid lines, while the results of numerical calculation are indicated by dotted lines. The calcium level increases more slowly in neurons with the short calcium decay time constant (40 ms) than in neurons with the long decay time constant (80 ms). This is also understood from Eq. (42). Error bars indicate the standard error of the mean (SEM).

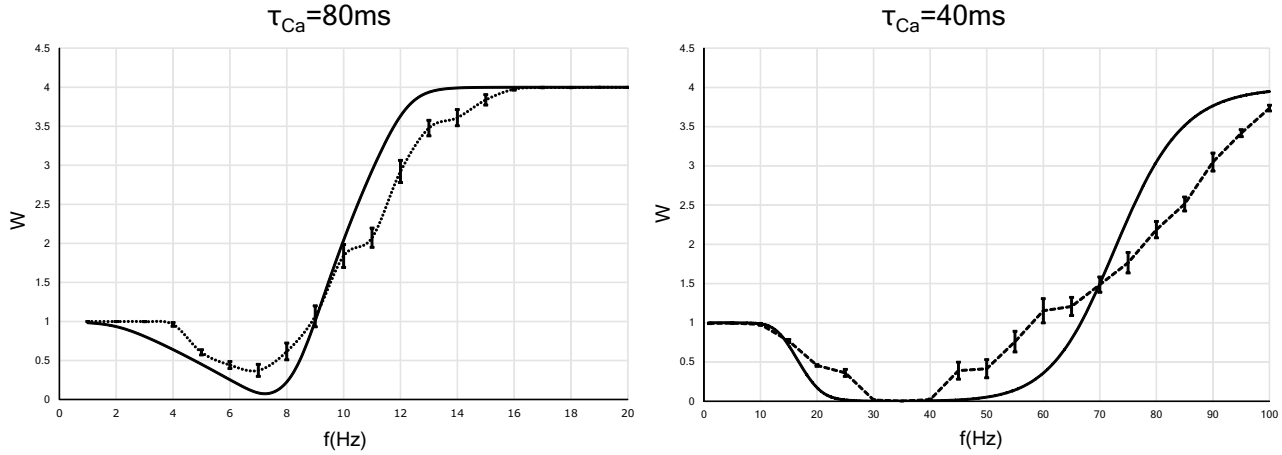

Figure 2. Synaptic strength in two types of neurons that have different calcium decay time constants as a function of the constant presynaptic stimulation frequency. The *x* axis indicates the input frequency, and the *y* axis represents normalized synaptic weights that are obtained after several hundreds of presynaptic spikes. The analytic solutions are indicated by solid lines, whereas the solutions provided by numerical calculation are indicated by dotted lines. Error bars indicate the SEM.

$$f = F^{-1}(Ca/\tau_{Ca}). \tag{1}$$

Equations (11) and (49) indicate that when the synaptic strength is at the LTD/LTP threshold, the postsynaptic calcium level has a fixed value:

$$Ca = \frac{1}{\beta}\log\frac{e^{\beta\alpha_1} - 0.25e^{\beta\alpha_2}}{0.75}. \tag{2}$$

Substituting the numerical values of the parameters in Eq. (11) into Eq. (2), we obtained $Ca = 0.54\,\mu M$. Thus, the stimulation frequency when the synaptic weight reaches the LTD/LTP threshold is a monotonically increasing function of $1/\tau_{Ca}$.

Postsynaptic calcium level and synaptic weight as functions of the average frequency of Poisson input. In several experimental studies on synaptic plasticity, the paradigms for inducing synaptic plasticity have consisted of constant-frequency stimulation trains, such as paired pulses or a tetanic stimulus. Neurons in vivo, however, are unlikely to experience such simple inputs. Rather, these neurons receive more complex input patterns in which ISIs are highly irregular[47]. The most representative stimulation patterns that are not constant-frequency stimulation trains are the Poisson process and the gamma process. In fact, spike sequences

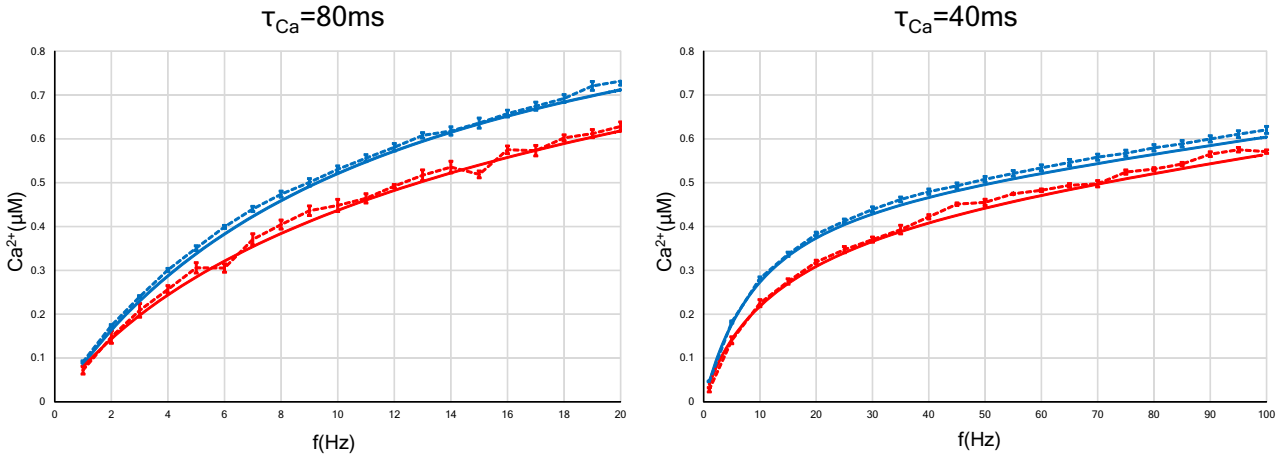

Figure 3. Relation between the postsynaptic calcium concentration and the average frequency of presynaptic constant-ISI (or Poisson) input. As in Fig. 1, two types of neurons with different calcium decay time constants were examined. The analytic solutions are shown with solid lines, whereas the results of numerical simulation are shown with dotted lines. The blue (or red) lines indicate the calcium concentration of the postsynapse with constant-ISI (or Poisson) input. In the case of Poisson input, the increase in calcium concentration with respect to the average frequency is slower than in the case of constant-ISI input. This result is independent of the calcium decay time constant. Error bars indicate the SEM.

similar to these processes are sometimes observed in neurons of brain[12,48–51]. In this section, we discuss the results for the FDP of neurons with Poisson-distributed spike trains.

First, the calcium concentration at the postsynapse receiving Poisson input was calculated numerically and is plotted with red dotted lines in Fig. 3, in which the calcium concentration with constant-ISI input is also plotted with blue dotted lines for comparison. In the same manner, we examined two kinds of neurons with calcium decay time constants of 40 ms and 80 ms. The intracellular calcium concentration, regardless of the stimulation pattern, increases more gradually in the case of $\tau_{Ca} = 40$ ms than in the case of $\tau_{Ca} = 80$ ms. Besides, the calcium level with Poisson input rises more slowly than that with constant-ISI input, which is independent of the calcium decay time constant (Fig. 3, left and right panels).

Here we discuss how the calcium concentration increases with the input frequency. In Eqs. (42) and (44), the first-half part $\tau_{Ca} f(\gamma_0 + \gamma_1 f + \gamma_2 f^2)$ is a supra-linear function of the stimulation frequency f. This part describes the approximate expression of the voltage-dependence of the postsynaptic events given by $H(V)$ in Eq. (14). The second-half parts $\sum_{j=f,s} I_j \tau_j \left[1 - \exp\left(-\frac{1}{\tau_j \cdot f}\right)\right]$ in Eq. (42) and $\sum_{j=f,s} I_j \frac{\tau_j}{\tau_j f + 1}$ in Eq. (44) converge to 0 in the limit of infinite f. Thus, the competition between the two parts determines whether the calcium concentration in Eqs. (42) and (44) increases sublinearly or supralinearly. As shown in Fig. S1, in cases of both constant-ISI and Poisson input, the calcium concentration increases sublinearly in the frequency range between 0 and approximately 100 Hz, which is usually observed in the brain[52]. This is because the second-half parts of Eqs. (42) and (44) are dominant in this frequency range. The effect of the first-half part becomes stronger as the input frequency increases above about 100 Hz, so that the calcium concentration increases supralinearly.

Next, we examined numerically the strength of a synapse receiving Poisson input. In Fig. 4, we define the LTD phase or LTP phase as the range of frequency indicating LTD or LTP. When the calcium decay time constant is 80 ms, interestingly, Poisson input makes the LTD phase disappear and the LTP phase is observed at any input frequency (see a dotted red line in Fig. 4, left panel), whereas in the case of constant-ISI stimulation, the LTD phase still exists at roughly between 3 and 9 Hz (see a dotted blue line in Fig. 4, left panel). When the calcium decay time constant is 40 ms, unlike in the case of $\tau_{Ca} = 80$ ms, changing the stimulus pattern from constant-ISI input to Poisson input shifted the LTD/LTP threshold to the right (see dotted blue and red lines in Fig. 4, right panel). Since the firing rate observed in the brain is found to be at most approximately 112 Hz, we need only consider synaptic plasticity within 100 Hz[52]. This consideration leads to the conclusion that Poisson input to a neuron with $\tau_{Ca} = 40$ ms expands the LTD phase and narrows the LTP phase. These results can be well reproduced by approximate analytical solutions [Eqs. (44) and (52)].

Analytical solutions for the calcium concentration with Poisson input [Eq. (44)] are plotted with red solid lines in Fig. 3, left and right panels. The solutions agree well with the numerical results(red dotted lines in Fig. 3) and indicate that Poisson stimulation gently increases the calcium concentration, as compared to constant-ISI input. This property does not depend on the calcium decay time constant (Fig. 5).

Next, we obtained an approximate expression for the relation between the synaptic weight and the average stimulation rate. By assuming that the synaptic weight $W(t)$ converges to a stationary solution in the long-time scale [Eq. (49)], we obtain Eq. (52). Solid lines in Fig 4 show that the analytical expression agrees well with the results of the numerical simulation. Regardless of the τ_{Ca} value, the synaptic weight varies slowly by changing the stimulus pattern from constant-ISI input to Poisson input. This change in the stimulation pattern moves the LTD/LTP threshold to the left and narrows the LTD phase decrease for $\tau_{Ca} = 80$ ms (see a solid red line in Fig. 4, left panel), whereas it has the opposite effect for $\tau_{Ca} = 40$ ms (see a solid red line in Fig. 4, right panel).

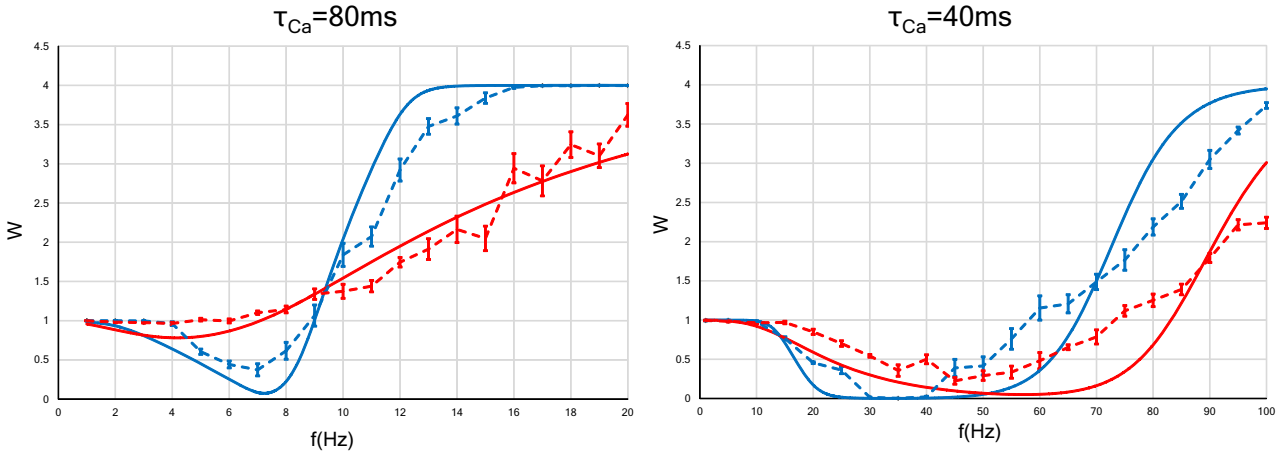

Figure 4. Synaptic strength for two types of neurons ($\tau Ca = 80$ ms and $\tau Ca = 40$ ms) as a function of the average rate of presynaptic stimulation. The x axis represents the input frequency, and the y axis represents normalized synaptic weights that are obtained after several hundreds of presynaptic spikes. The analytic solutions are shown with solid lines, whereas the results of numerical simulation are shown with dotted lines. Error bars indicate the SEM. The blue (or red) lines indicate the synaptic weights with constant-ISI (or Poisson) input. The synaptic weight with the Poisson input changes slowly compared to that with the constant-ISI input. As shown by the numerical simulation results, in neurons with $\tau Ca = 80$ ms, the Poisson input makes the LTD phase disappear, and only the LTP phase remains (a red dotted line in left panel). On the other hand, in neurons with $\tau_{Ca} = 40$ ms, the LTD/LTP threshold moves to the right, and the LTD phase increases (red dotted line in right panel). These results are also qualitatively illustrated by analytical solutions (solid lines).

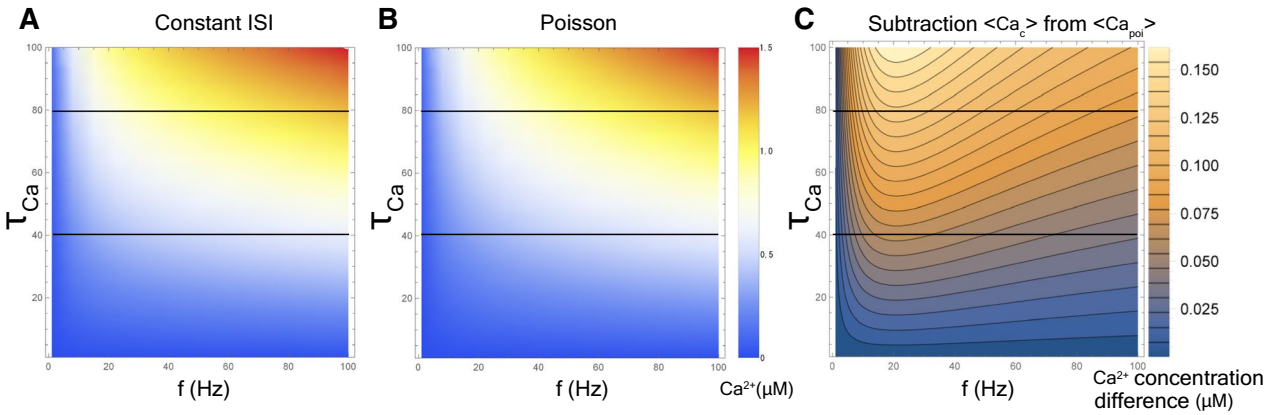

Figure 5. Two-dimensional density plot of post-synaptic calcium concentration as a function of f and τ_{Ca}. We illustrate the calcium concentration with the constant-ISI input expressed in Eq. (42) (**A**) and with the Poisson input expressed in Eq. (44) (**B**). (**C**) Density plot of $\langle Ca_c(f, \tau_{Ca})\rangle - \langle Ca_{poi}(f, \tau_{Ca})\rangle$. The horizontal lines on each figure suggest corresponding values at $\tau_{Ca} = 40$ ms and $\tau_{Ca} = 80$.

Thus, the numerical and analytical studies indicate that the postsynaptic calcium concentration and synaptic strength receiving Poisson input behave differently from those receiving constant-ISI stimulation. At the same frequency, when $\tau_{Ca} = 80$ ms, a synapse receiving Poisson input is more likely to be LTP than a synapse receiving constant-ISI input, and when $\tau_{Ca} = 40$ ms, a synapse receiving Poisson input is more likely to be LTD. These findings suggest that the difference in input patterns (constant-ISI or Poisson input) and calcium decay time constant affects the output of FDP, i.e., LTD or LTP. In addition, this tendency to become LTP or LTD by changing the input pattern depends on the postsynaptic calcium decay time constant.

Postsynaptic calcium level and synaptic weight as a function of the average frequency of gamma process input. We studied the postsynaptic calcium concentration and synaptic load of neurons receiving gamma process inputs, which is one of the firing patterns observed in brain[51,53]. Since the analytic solutions are qualitatively consistent with the simulation results so far presented in the present paper, we discuss the plasticity of synapses receiving gamma process input by only the analytic solutions. The postsynaptic calcium concentration of neurons that receive gamma process input is expressed by Eq. (48), where α is a shape parameter. The synaptic weight of the neurons receiving gamma process input is approximately expressed by Eq. (53) as a function of average input frequency.

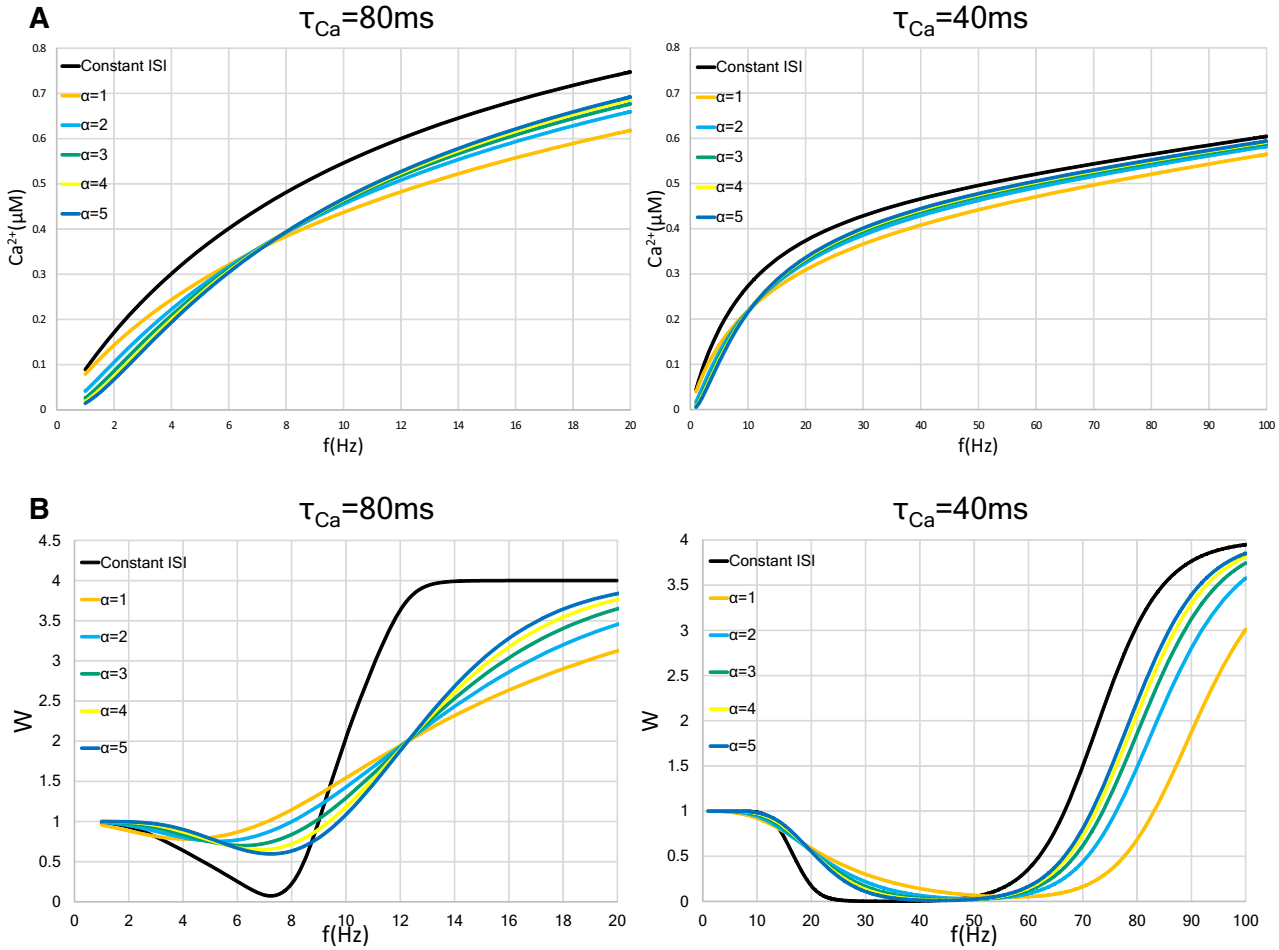

Figure 6. Change in the postsynaptic calcium concentration and the weight in the synapse with gamma process input. We show two types of neurons with different time constants of calcium decay, $\tau_{Ca} = 80$ ms and 40 ms. In each graph, the black, orange, light blue, blue green, yellow, and blue lines indicate constant-ISI input, shape parameter $\alpha = 1, \alpha = 2, \alpha = 3, \alpha = 4$, and $\alpha = 5$, respectively. (**A**) Relationship between the postsynaptic intracellular calcium concentration and input frequency f in neurons stimulated with gamma process input. A graph of constant-ISI stimulation is shown as a control (black lines). The trace of the shape parameter $\alpha = 1$ matches the graph of the Poisson input. As the value of the shape parameter increases, the calcium level increases is faster. (**B**) Approximate relationship between synaptic weight and mean input frequency in neurons with constant-ISI and gamma process inputs. The LTD/LTP threshold moves to a higher frequency in the case of $\tau_{Ca} = 80$ ms and the moves lower in the case of $\tau_{Ca} = 40$ ms as the value of the shape parameter becomes large.

This result for the calcium concentration is illustrated in Fig. 6A. As the shape parameter increases, the slope of the calcium concentration increases. The results for the synaptic weight are shown in Fig. 6B. When neurons with $\tau_{Ca} = 80$ ms are stimulated by gamma process input, as the shape parameter α increases, the LTD/LTP threshold shifts to a higher frequency and the minimum value of the synaptic weight becomes smaller (Fig. 6B, left). When $\tau_{Ca} = 40$ ms, the LTD/LTP threshold shifts to a lower frequency as the shape parameter α increases; on the other hand, the minimum value of the synaptic weight is approximately the same from $\alpha = 1$ to $\alpha = 5$ (Fig. 6B, right).

In summary, the postsynaptic calcium level with gamma process input increases slower than that with constant-ISI input, but increases faster than that with Poisson input. As the shape parameter increases, the increase in the calcium concentration becomes faster. The tendency to induce LTP or LTD by gamma process input depends on the shape parameter. These results suggest that the difference in input pattern as well as the shape parameter in gamma process input affects the synaptic weight.

Effect of increase in background synaptic activity receiving constant-ISI input. The postsynaptic terminals in neurons in vivo display intense background activity, which is characterized by fluctuations in the postsynaptic membrane potential. This background activity has at least three components: dendritic action potential, BPAPs, and voltage noise[41,54]. The voltage noise includes the stochastic properties of ion channels, the random release of neurotransmitter, and thermal noise. The distance from the soma or the differences in the cortical layer, in which neurons are located, affects the frequency and size of the amplitude of the background synaptic activity[38–40].

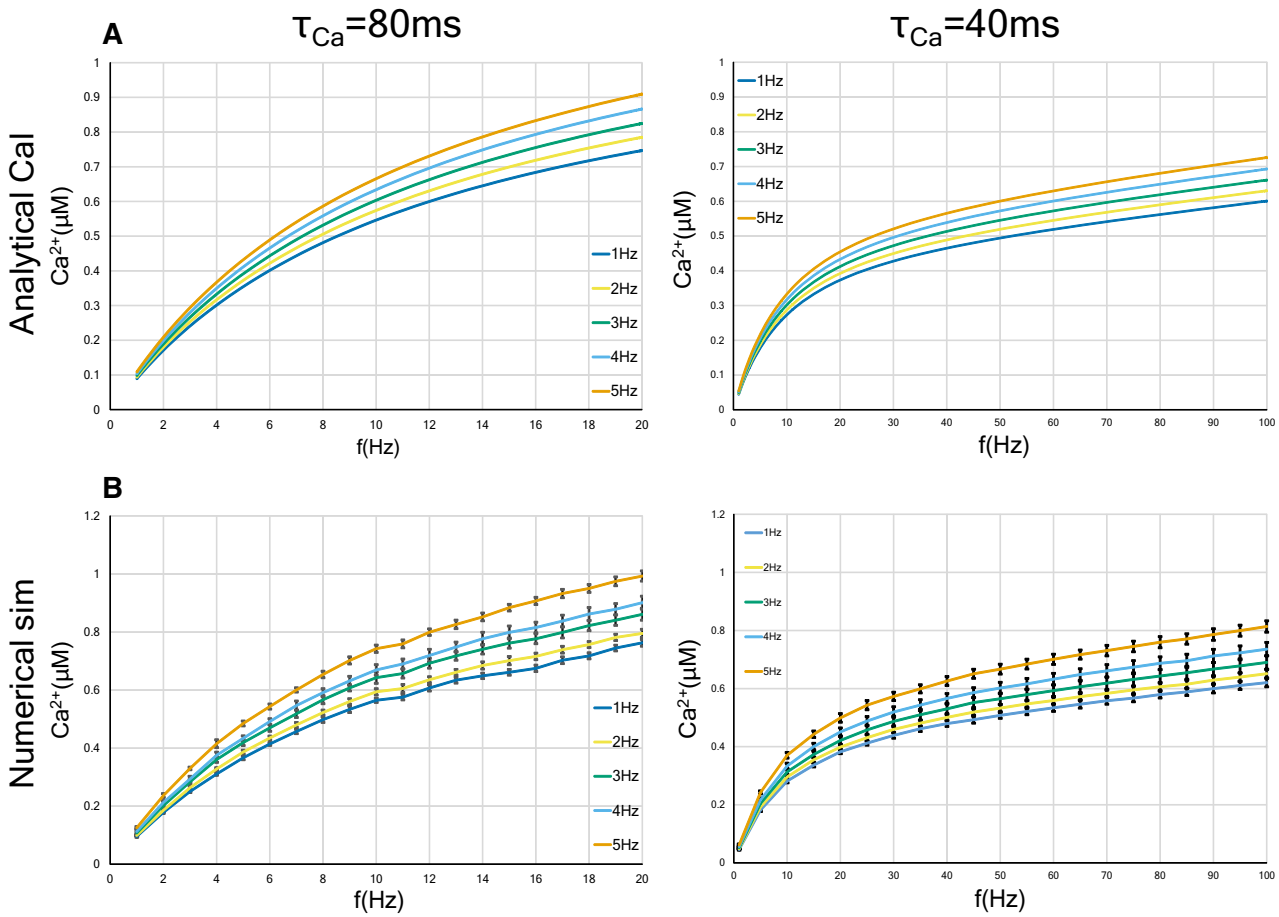

Figure 7. Postsynaptic calcium concentration in two types of neurons ($\tau Ca = 80$ ms and $\tau Ca = 40$ ms) as a function of the frequency of presynaptic input and of the background input. The ISI of the presynaptic input is constant. The background Poisson input with a frequency in the range of 1 to 5 Hz was applied. The analytic solution is shown in (**A**), whereas the results of numerical simulation are shown in (**B**). Error bars indicate the SEM.

In order to examine the FDP under various background synaptic activities, we first analytically and numerically calculated the dependence of the postsynaptic calcium concentration on the constant-ISI input under various frequencies of background Poisson input. The fluctuation of the membrane potential due to background synaptic activity is denoted by V_{bg} in Eq. (18). Since V_{bg} increases in proportion to the average frequency of the background synaptic activity f_{bg}, $H(V)$ in Eq. (37) is approximately expressed as a bivariate quadratic function of f and f_{bg}. Thus, the postsynaptic calcium concentration is given as a function of f and f_{bg} as follows:

$$\left\langle Ca_c(f, f_{bg}) \right\rangle = \tau_{Ca} f(\zeta_0 + \zeta_1 f + \zeta_2 f_{bg} + \zeta_3 f^2 + \zeta_4 f f_{bg} + \zeta_5 f_{bg}^2) \sum_{j=f,s} I_j \tau_j \left[1 - \exp\left(-\frac{1}{\tau_j \cdot f} \right) \right], \tag{3}$$

where $\zeta_0 = 1.21 \times 10^{-2}$, $\zeta_1 = 2.97 \times 10^{-5}$, $\zeta_2 = 6.12 \times 10^{-4}$, $\zeta_3 = 3.52 \times 10^{-8}$, $\zeta_4 = 1.45 \times 10^{-6}$, and $\zeta_5 = 1.49 \times 10^{-5}$. Figure 7A plots Eq. (3) using $\tau_{Ca} = 80$ ms or $\tau_{Ca} = 40$ ms. In both cases, the higher the average frequency of the background Poisson input is, the faster the rate of increase in the calcium concentration with synaptic input frequency becomes. As shown in Fig. 7B, qualitatively consistent results were obtained by numerical simulations.

We next analytically and numerically calculated the relation between the synaptic weight and the input frequency under various background input rates. The approximate analytic solution is obtained as follows:

$$\left\langle W_c(f, f_{bg}) \right\rangle = \int_0^\infty dx \int_0^1 d\epsilon \; \delta(1 - x) \Omega(Ca_c(f, f_{bg}, x, \epsilon | r_{Ca;c}, r_{j;c})). \tag{4}$$

Here, $Ca_c(f, f_{bg}, x, \epsilon | r_{Ca;c}, r_{j;c})$ is defined by Eq. (3) in Eq. (50). More explicitly, $Ca_c(f, f_{bg}, x, \epsilon | r_{Ca;c}, r_{j;c})$ is given by

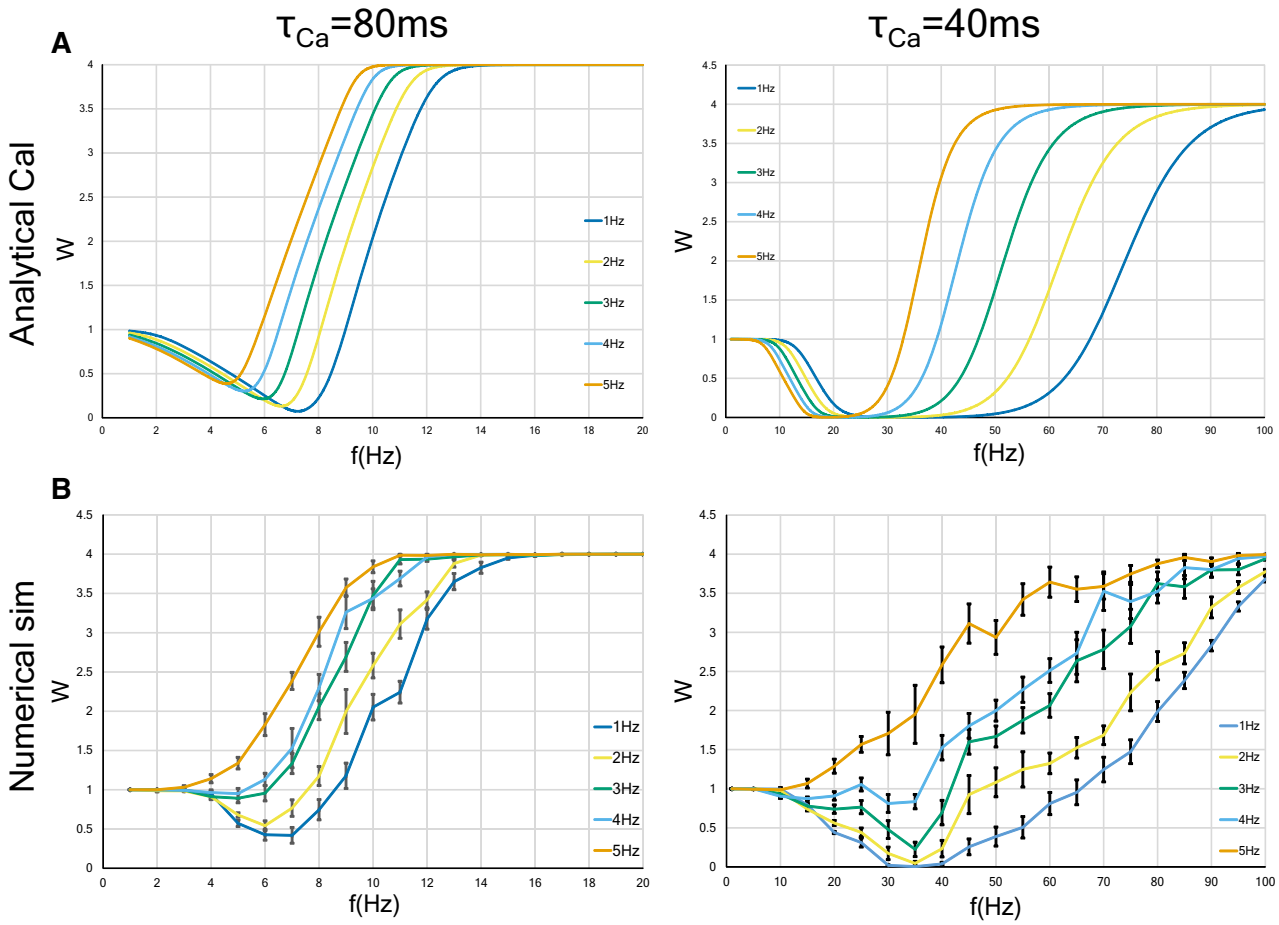

Figure 8. Synaptic strength as a function of the frequency of presynaptic constant-ISI input and of the background Poisson input, under the background Poisson input with a frequency in the range of 1 to 5 Hz. Two types of neurons ($\tau_{Ca} = 80$ ms and $\tau_{Ca} = 40$ ms) were examined. The analytic solution and the results of numerical calculation are shown in A and B, respectively. Error bars indicate the SEM.

$$
\begin{aligned}
&Ca_c(f, f_{bg}, x, \epsilon | r_{Ca;c}, r_{j;c}) \\
&= (\zeta_0 + \zeta_1 f + \zeta_2 f_{bg} + \zeta_3 f^2 + \zeta_4 f f_{bg} + \zeta_5 f_{bg}^2) \sum_{j=f,s} I_j \tau_{0j} \left\{ \exp\left(-\frac{\epsilon}{\tau_{jf}}\right) - \exp\left(-\frac{\epsilon}{\tau_{Caf}}\right) \right. \\
&+ \left. \exp\left(-\frac{\epsilon}{\tau_{Caf}}\right) \left[\exp\left(-\frac{x}{\tau_{jf}}\right) - \exp\left(-\frac{x}{\tau_{Caf}}\right) \right] + \exp\left(-\frac{x+\epsilon}{\tau_{Caf}}\right) \left(\frac{r_j - r_{Ca}}{1 - r_{Ca}}\right) \right\}.
\end{aligned} \tag{5}
$$

The analytical solution (4) is plotted in Fig. 8A, and the corresponding numerical solution is shown in Fig. 8B. Although the analytical solution captures the overall qualitative behavior of the numerical solution, one can see quantitative deviations. These deviations can be attributed to the fact as follow. First, as you can see from Eq. (16), the time fluctuation of the postsynaptic membrane potential $V(t)$ elevates as the background input increases. Accordingly, the time dependence of $H(V)$ in Eq. (14) or Eq. (20) cannot be ignored, which leads to the difficulty in establishing "Assumption 1" (see the "Methods" section). Second, as shown in the description of Eq. (42) in the "Methods" section, $H(V)$ is approximated by a quadratic power series around the resting membrane potential. Therefore, when V moves away from the resting potential due to an increase in background activity, the approximation accuracy of $H(V)$ deteriorates.

Although two types of neurons with different calcium decay time constants were examined, the influence on the synaptic strengths by the increase of the background input level is qualitatively common to both types of neurons. In other words, the increase in the background input rate moves the LTD/LTP threshold to the left, decreases the LTD phase, and broadens the LTP phase.

Thus, upregulation of background synaptic activities leads to the enhancement of synaptic efficacy through the acceleration of the increasing rate of postsynaptic calcium concentration. These results suggest that the FDP output (LTP or LTD) varies depending on the magnitude of the applied background noise, even if the input frequency is the same.

We summarize the findings of the present study: (1) We obtained approximately analytical solutions of the intracellular calcium concentration and the synaptic weight as a function of the frequency of three kinds of

input: constant-ISI, Poisson, and gamma process input. The latter two input patterns are often observed in vivo. (2) In all three input patterns, LTP occurs at a lower frequency as the calcium decay time constant increases. We used 80 ms as the longer calcium decay time constant ($= \tau_{Ca}$) and 40 ms as the shorter calcium decay time constant. (3) The intracellular calcium level increases more slowly in neurons with Poisson input than in neurons with constant-ISI input. At the same stimulation frequency, a synapse with a long calcium decay time constant tends to be strengthened (LTP) by changing the stimulation pattern from constant-ISI input to Poisson input, while a synapse with a short calcium decay time constant weakened (LTD). (4) The calcium level with gamma process input increases faster than that with Poisson input but slower than that with constant-ISI input. Moreover, calcium level with gamma process also increases faster as the shape parameter grows. As the shape parameter increases, the LTD/LTP threshold moves to a higher frequency in $\tau_{Ca} = 80$ ms neurons but moves to a lower frequency in $\tau_{Ca} = 40$ ms neurons. The minimum value of the synaptic weight is smaller in $\tau_{Ca} = 80$ ms neurons but is approximately constant in $\tau_{Ca} = 40$ ms neurons as the shape parameter increases. (5) The increase of background synaptic activities induces the acceleration of the increase rate of the calcium level and the enhancement of synaptic weight.

Discussion

The Shouval's model we studied is the most pioneering calcium-based model and is biophysically valid[33,55]. However, this model is quite complicated for analytical study. In the present study, focusing on only the long-term behavior of postsynaptic events, we derived approximate-analytic solutions from the Shouval's model. Our results found from the analytic solutions indicate that the synaptic weight by FDP depends not only on input frequency but also on input pattern, shape parameter in gamma process input, calcium decay time constant, and background synaptic activity, which have been suggested to vary in vivo depending on the location, the internal state, and the external environment of the neuron[41–43,51,53,54].

We now discuss the relevance of our study to some related prior works. Interestingly, conclusions similar to ours have been obtained from studies of some STDP models, which considered not intracellular mechanisms but only spike timing. The triplet-based model of STDP, which is much simpler than the Shouval's model that was the basis of our research, explained the BCM rule and derived a similar conclusion to our Fig. 4, left panel, that is changing from regular to irregular spike patterns tends to evoke LTP[20,56]. Why are similar conclusions drawn from disparate models? Although all variables in equations of the triplet-based model are not identified as specific biophysical quantities, it is suggested that variables $o1$ and $o2$ in Eq. (2) in Pfister and Gerstner, 2006[56] may be related to the calcium current depending on the post-synaptic membrane potential, and the dynamics of the latest and second-to-latest spikes are considered. On the other hand, as can be seen from the Eqs. (23), (24) and (25), we separately calculated the contribution from the latest spike ($= H(V)(T_N^f + T_N^s)$) and the contribution from all previous spikes ($= H(V)(S_{N-1}^f + S_{N-1}^s)$), when analysing the calcium influx in the postsynapse depending on membrane potential. The triplet model seems to ignore the effect of the spikes other than the latest and second-to-latest ones. However, they decay exponentially quickly, and thus although these two studies differ in how far past spikes are calculated, they may be both good approximate representations of the post-synaptic events. Also, the results of the STDP model taking into account dendritic and axonal propagation delays, reported by Madadi Asl et al. do not contradict ours[26,27]. They showed that, in both two-neuron and network motifs, high-frequency firings promote bidirectional connections, indicating a large proportion of neurons with large synaptic weights. Low-frequency firings lead to unidirectional or decoupled connections, showing the decrease of the mean synaptic weight. These findings are similar to the BCM curve in the FDP (Fig. 2) and the induction of LTP by the increase in background postsynaptic inputs (Fig. 8B).

Graupner et al. proposed a calcium-based model that simplifies the Shouval's model. They found that differences in plasticity outcomes are due to differences in parameters defining the calcium dynamics[29]. We have similar conclusions in this study; that is, LTP tends to occur even at a lower frequency as the calcium decay time constant increases (Fig. 2). Besides, applying firing patterns recorded in monkey area MT to the triplet-based model and the simplified calcium model, they found that synaptic plasticity can occur sufficiently with only the variation of firing rate without exact spike timing[20]. Furthermore, they investigated the effect of irregular input patterns on long-term plasticity with these models. They showed that irregular spike pairs tend to induce potentiation more than regular spike pairs. This conclusion is also similar to that obtained in this paper, that is, in $\tau_{Ca} = 80$ ms neurons, changing from constant-ISI to Poisson input makes LTP easy to be induced (Fig. 4, left panel).

In addition to these conclusions, we obtained the following new findings. First, we found that Poisson stimulation evokes a lower calcium concentration than constant-ISI stimulation for the same input frequency (Figs. 3 and 5C). At a glance, this finding may appear counterintuitive, because, in the case of Poisson input, the probability of firing in the period between 0 ms and the time of average ISI is $1 - 1/e$. It indicates that the proportion of firing with an ISI shorter than the average ISI is higher compared to that of firing with an ISI longer than the average ISI. However, the result we obtained is the opposite. To elucidate the reason for this, we obtained analytic solutions of the statistical average of the calcium current through NMDA receptor under constant-ISI and Poisson input as follows:

$$\left\langle I_{\mathrm{c,\,NMDA}}(f)\right\rangle = f(\gamma_0 + \gamma_1 f + \gamma_2 f^2)\sum_{j=f,s} I_j \tau_j \left[1 - \exp\left(-\frac{1}{\tau_j \cdot f}\right)\right], \tag{6}$$

$$\left\langle I_{\text{poi, NMDA}}(f)\right\rangle = (\gamma_0 + \gamma_1 f + \gamma_2 f^2) \sum_{j=f,s} I_j \frac{\tau_j f}{\tau_j f + 1}. \tag{7}$$

We also define the subtraction of Eq. (7) from Eq. (6) as follows:

$$\Delta\left\langle I_{\text{NMDA}}(f)\right\rangle := \left\langle I_{\text{c, NMDA}}(f)\right\rangle - \left\langle I_{\text{poi, NMDA}}(f)\right\rangle, \tag{8}$$

In Fig. S2, we plot the analytical solution of $\Delta\left\langle I_{\text{NMDA}}(f)\right\rangle$ in Eq. (8). Equations (8) and (13) indicate that, at any input frequency, the Poisson input leads to a smaller I_{NMDA} than the constant-ISI input, resulting in a smaller calcium concentration. For Poisson input, when firing with ISIs longer than the average, V_{epsp} (EPSPs generated by binding glutamate to the AMPA receptors) and I_{NMDA} might decay much stronger than the case of firing with ISIs shorter than the average [cf. Eq. (17) and Eq. (20)].

Second, as can be seen from Eq. (1), where F^{-1} is a monotonically increasing function, we found that the LTD/LTP threshold under constant-ISI input can be written as a monotonically increasing function of $1/\tau_{Ca}$. Moreover, we showed that the LTD/LTP threshold by changing from regular to irregular spikes shifts to lower frequency when τ_{Ca} is long (Fig. 4, left panel) and to higher frequency when τ_{Ca} is short (Fig. 4, right panel). It is necessary to examine whether the difference in the changes in the LTD/LTP threshold due to the calcium decay time constant is found in other calcium models such as the simplified calcium model and whether this phenomenon actually occurs in the brain.

For a long time, there has been a debate on the nature of neural coding, which is primarily founded on the generation, propagation, and processing of spikes[57–59]. The classical view of neural coding emphasizes the information carried by the rate at which neurons produce action potentials, whereas spike variability and background activity were ignored or treated as noise[28,60,61]. In experimental and theoretical studies of recent decades, arguing the importance of the spike timing rather than the firing rate in neural coding, the spike variability and background activity are also considered as noise activities[12,25]. However, the results of recent electrophysiological experiments on waking animals suggest that they are too large to be ignored for precise spike timing[25,54], leading to a renewed awareness of the importance of the rate coding, which is less affected by individual spike variability and background noise[20,21]. Moreover, recent studies reveal the need for several simultaneous codes (multi-coding), including spike variability and fluctuation of membrane potential, as sources[57,62–64]. Hence, the multi-coding hypothesis for the neural coding problem may be supported by the results of the present study, suggesting that not only firing rate but also firing variability, the internal parameters of neurons, and the magnitude of background synaptic activity could be important for neural coding and synaptic plasticity[28,57].

We found that the calcium decay time constant determines the plasticity outcome. In neurons with a long time constant, LTP is induced even by a small presynaptic rate (about 9 Hz), because the calcium concentration via the NMDA receptors increases faster in these neurons than in neurons with a short time constant (Figs. 1 and 2). In neurons with a short time constant, LTP is not induced until the stimulation frequency is large (over about 50 Hz). This difference due to calcium dynamics is more pronounced when the stimulation pattern is set to Poisson or gamma process input (Figs. 4 and 6).

The calcium decay time constant is closely related to the function of sodium-calcium exchangers (NCXs)[65]. Sodium-calcium exchangers, which are expressed highly in dendrites and dendritic spines in a variety of brain regions[66], are controlled in activity by various intracellular and extracellular signaling molecules[67] and are widely involved in many neural events from developmental processes to cognitive abilities[68,69]. Thus, the calcium decay time constant differs depending on anatomical and physiological characteristics. Indeed, previous reports suggest that the calcium decay time constant varies with the depth of the cerebral cortex and that nitric oxide stimulates the increase of the calcium decay time constant in a cGMP-dependent manner[43,67,70]. Our findings and those of previous studies suggest that, even with the same frequency, the synaptic plasticity induced thereby depends on the anatomical and physiological factors and that this difference becomes more prominent when the stimulation pattern is irregular.

Previous studies have demonstrated that applying an appropriate level of noise to the postsynapse results in the enhancement of the neural sensitivity and the improvement of signal detection in the central nervous system[71,72]. Consistent with these findings, our research indicates that increased synaptic noise is more likely to induce LTP, regardless of the calcium decay time constant. Recently, the dendritic action potential has been considered as one of the main components of synaptic noise. In the record of the dendritic membrane potential of freely behaving rats, dendrite spikes accompanied by large subthreshold membrane potential fluctuations occur with high rates greater than the BPAP evoked in the soma[54]. In addition, it has been shown in hippocampal synapses that even a single presynaptic burst induces LTP, provided dendritic action potentials are generated[73]. These findings and our results indicate that inputs from other than the presynapse, such as background synaptic activity, including the BPAP and the dendritic action potential, are largely involved in synaptic plasticity, especially the generation of LTP. We cannot, however, conclude from our results that even a single presynaptic input induces LTP. It is necessary to conduct research in which single-burst-induced LTP is substantiated experimentally. Therefore, a mathematical model that further improves the model used in the present study should be constructed.

Our study has the limitations as follows: (1) This study is a model study without experiments. By solving the Shouval's model under various conditions analytically and numerically, we obtained conclusions that are similar to or novel over the previous studies. However, they are merely theoretical predictions, and whether they occur in the brain has to be verified by future experiments. (2) Since we analyzed only the long-term behavior of the Shouval's model, the transient nature of synaptic plasticity in vivo was ignored. (3) Since our research uses the Shouval's model, which considers only post-synaptic plasticity, we do not examine the presynaptic factors. However, in 2015, a new model of spike timing plasticity was proposed by Rui Ponte Costa et al. in which both

pre- and post-synaptic plasticity were considered (referred to as "pre-post STDP model")[74]. They used Poisson input as input pattern and showed that the pre-post STDP model induces higher SNR (signal-to-noise ratio) of a synaptic response than models considering only post-synaptic changes, and induces fast re-learning of stimuli experienced in the past. Therefore, it may be more appropriate to investigate, considering the pre- and post-synaptic plasticity, the influence on the synaptic weight by a difference in spike pattern, calcium dynamics, and background activity. It is necessary to clarify this point in the future. (4) We did not investigate the involvement of higher-order correlations. Gjorgjieva et al. analyzed the triplet-based model of STDP analytically and numerically[55]. They showed that, even when the input frequency is constant, the difference in spatial and spatiotemporal correlations determines the synaptic weight. It is a future task to study calcium dynamics and weight dynamics with highly correlated inputs to the calcium-based model. (5) We used only one model. It will be possible to deepen an understanding of synaptic plasticity by performing similar analysis as done in this paper on other mathematical models, STDP models and calcium models.

In conclusion, a problem regarding the FDP, namely, a firing rate abstraction, in which the temporal average of spikes is taken, is discussed, ignoring a large amount of extra information within the encoding window, such as the variation of firing pattern[3,28,61]. This loss of information contrasts the encoding of rapidly changing neuronal activity observed in the brain[3,28]. The present study showed theoretically that the output of synaptic plasticity in neurons receiving the same input frequency differs depending on the input pattern, the calcium decay time constant, and the background activity, which are related by neuron type and the anatomical and physiological condition in the brain. This finding suggests that information neglected in the view that only the firing rate induces the synaptic plasticity is also involved in the synaptic plasticity and neural coding. In the future, the ratio at which this information is related to synaptic plasticity and neural coding should be verified experimentally and theoretically.

Methods

Model. We used a model for the FDP based on the calcium control hypothesis of Shouval et al., assuming that the change of the synaptic weight is fully determined by the postsynaptic calcium level[33,44].

The dynamics of the synaptic weight $W(t)$ are governed by

$$\frac{d}{dt}W(t) = \eta(Ca(t))[\Omega(Ca(t)) - W(t)], \tag{9}$$

where $Ca(t)$ represents the intracellular calcium concentration, and η and Ω are functions of intracellular calcium concentration given by the following formulas:

$$\eta(Ca) = \left[\frac{p1}{p2 + (Ca)^{p3}} + p4\right]^{-1}, \tag{10}$$

$$\Omega(Ca) = 1 + 4\mathrm{sig}(\mathrm{Ca} - \alpha_2, \beta_2) - \mathrm{sig}(\mathrm{Ca} - \alpha_1, \beta_1), \tag{11}$$

where

$$\mathrm{sig}(\mathrm{x}, \beta) = \exp(\beta \mathrm{x})/[1 + \exp(\beta \mathrm{x})], \tag{12}$$

and we used the following parameters: $p1 = 0.1$ s, $p2 = p1/10^{-4}$, $p3 = 3$, $p4 = 1$ s, $\alpha_1 = 0.35\,\mu\mathrm{mol/dm}^3$, $\alpha_2 = 0.55\,\mu\mathrm{mol/dm}^3$ and $\beta_1 = \beta_2 = 80\,\mu\mathrm{mol/dm}^3$[33,44].

The dynamics of the intracellular calcium concentration are described as follows:

$$\frac{d}{dt}Ca(t) = I_{\mathrm{NMDA}}(t) - \frac{1}{\tau_{ca}}Ca(t), \tag{13}$$

where τ_{ca} is the calcium decay time constant. In order to investigate the relation between the calcium dynamics and the synaptic plasticity, we examined two kinds of neurons with time constants of 40 ms and 80 ms, which are known as representative values in pyramidal cells in the superficial cortex (layers II to IV) and the deep cortex (layers V to VI)[42,43].

In Eq. (13), I_{NMDA} represents the calcium current via the NMDA receptor and is expressed as a function of time and postsynaptic potential as follows:

$$I_{\mathrm{NMDA}}(t, V) = H(V)\left[I_f \Theta(t) e^{(-t/\tau_f)} + I_s \Theta(t) e^{(-t/\tau_s)}\right]. \tag{14}$$

Here, $\Theta(t)$ is the Heaviside step function and we choose the parameters $I_f = 0.75$, $I_s = 0.25$, $\tau_f = 50$ ms, and $\tau_s = 200$ ms, and $H(V)$ is given by

$$H(V) = -P_0\, G_{\mathrm{NMDA}} \frac{(V - V_r)}{1 + (Mg/3.57)\exp(-0.062V)}, \tag{15}$$

where we choose the parameters $P_0 = 0.5$, $G_{\mathrm{NMDA}} = -1/140\ \mu\mathrm{mol\ dm}^{-3}/(\mathrm{m\,mV})$, $Mg = 3.57$, and a reversal potential for calcium ions of $Vr = 130$ mV[33]. Since $H(V)$ increases monotonically with the membrane potential V before reaching a plateau at $V = 27.1$ mV, the higher the membrane potential the greater the calcium current through the NMDA receptor, I_{NMDA}, as long as $V < 27.1$ mV.

The postsynaptic membrane potential is given as the sum of the resting membrane potential V_{rest}, which is set to −65 mV, and the depolarization terms $V_{\mathrm{epsp}} + V_{\mathrm{bg}}$:

$$V(t) = V_{\mathrm{rest}} + V_{\mathrm{epsp}}(t) + V_{\mathrm{bg}}(t). \tag{16}$$

The depolarization terms in Eq. (16) include both EPSPs generated by binding glutamate to the AMPA receptors ($= V_{\mathrm{epsp}}$) and background contribution ($= V_{\mathrm{bg}}$), which describes the depolarization due to the factors other than EPSP. Here, V_{epsp} is expressed as

$$V_{\mathrm{epsp}}(t) = \sum_i \Theta(t - t_i)\left[e^{-(t-t_i)/\tau_1} - e^{-(t-t_i)/\tau_2}\right], \tag{17}$$

where t_i indicates the i-th presynaptic spike time, and the time constants are $\tau_1 = 50$ ms and $\tau_2 = 5$ ms[33]. Here, V_{bg} is composed of the summation of the dendritic action potentials, the back propagating action potentials (BPAPs), and the voltage noise applied to the postsynapse. The amplitude of the depolarization generated at the postsynaptic dendritic spine by the BPAPs varies, decreasing exponentially with the distance from the soma, at which it is about 100 mV relative to the synapse[40,75]. The duration of the depolarization by BPAPs also differs among cell types[76]. Moreover, the noise level at dendritic spines has been reported to be similar to that measured at the soma[77]. We took these previous studies into consideration in order to perform the numerical simulation and presumed that the spike trains by both BPAPs and voltage noise follow a homogeneous Poisson process. Thus, we simply expressed V_{bg} as follows:

$$V_{\mathrm{bg}}(t) = s\sum_k \Theta(t - t_k)\left[e^{-(t-t_k)/\tau_1} - e^{-(t-t_k)/\tau_2}\right], \tag{18}$$

where $s = 20$ mV and $\{t_k\}$ is a Poisson process with a frequency that varies depending on the simulation conditions. (In all simulations except for those of Figs. 7 and 8, we used a Poisson process with a mean frequency of 1 Hz.)

Numerical simulations. In the present study, we performed numerical simulations as well as analytical calculations in order to investigate the FDP. We used Wolfram Mathematica software in all simulations, and determined the dependence of both the calcium concentration and the synaptic weight on the stimulation frequency as follows. First, we repeatedly solved Eqs. (9)–(18) numerically as a function of time for each frequency. The calcium concentration as a function of time obtained by this calculation is similar to the results of a previous paper[46]. Next, after a period of 8.5×10^4 ms, which is necessary for the system to reach a steady state, the average of the calcium level or the synaptic efficacy between 8.5×10^4 ms to 9.0×10^4 ms was calculated. When simulating with Poisson inputs, we performed the above calculations for at least three input patterns by changing the random seed, and took the average. The quantitative data are expressed as the mean of ten independent experiments plus/minus the standard error of the mean (SEM).

Derivation of the analytic solutions of the postsynaptic calcium concentration as functions of the average frequency of constant-ISI, Poisson, and gamma process inputs. By integrating Eq. (13), we can formally express the solution for $Ca(t)$ as

$$Ca(t) = \int_0^t e^{\frac{1}{\tau_{ca}}(s-t)} I_{\mathrm{NMDA}}(s)ds. \tag{19}$$

Considering that the ion current through NMDAR (I_{NMDA}) is reset to zero each time presynaptic input is applied, Eq. (14) is rewritten as follows for the interval between the presynaptic inputs $\hat{t}_k \le s \le \hat{t}_{k+1}$, where $\hat{t}_k$ is the time for k-th presynaptic input ($\hat{t}_0 = 0$ ms):

$$\begin{aligned} I_{\mathrm{NMDA}}(s) = H(V)\Big[&I_f\Theta(s - \hat{t}_k)e^{-(s-\hat{t}_k)/\tau_f} \\ &+ I_s\Theta(s - \hat{t}_k)e^{-(s-\hat{t}_k)/\tau_s}\Big]. \end{aligned} \tag{20}$$

Now, we make the following assumptions.

Assumption 1 The time dependence of $H(V)$ can be neglected because it varies slowly in time compared to the other terms in Eq. (20)

Assumption 2 The spike interval fluctuates stochastically. If we define the average spike interval as Δt, $\hat{t}_k$ is written as follows:

$$\hat{t}_k = \delta_k \Delta t + \hat{t}_{k-1}, \quad \hat{t}_0 = 0. \tag{21}$$

Then,

$$\hat{t}_k = \sum_{k'=1}^{k} \delta_{k'} \Delta t \quad (k \geq 1). \tag{22}$$

Inserting Eq. (20) into Eq. (19) with Assumption 1, we obtain

$$\begin{aligned} Ca(t) =& H(V) \sum_{k=0}^{N} \int_{\hat{t}_k}^{\hat{t}_{k+1}} ds \Big[I_f \Theta(s - \hat{t}_k) e^{-(s-\hat{t}_k)/\tau_f} \\ &+ I_s \Theta(s - \hat{t}_k) e^{-(s-\hat{t}_k)\tau_s} \Big] e^{\frac{1}{\tau_{ca}}(s-t)} \\ =& H(V)[S^f_{N-1}(t) + T^f_N(t) + S^s_{N-1}(t) + T^s_N(t)], \end{aligned} \tag{23}$$

where we have separated the contributions from the N-th presynaptic input, $T^f_N(t)$ and $T^s_N(t)$ from the contributions from the first $N-1$ presynaptic inputs, $S^f_{N-1}(t)$ and $S^s_{N-1}(t)$:

$$S^j_{N-1}(t) := \sum_{k=0}^{N-1} \int_{\hat{t}_k}^{\hat{t}_{k+1}} ds\, I_j\, e^{-\frac{1}{\tau_j}(s-\hat{t}_k)}\, e^{\frac{1}{\tau_{Ca}}(s-t)}, (j = f \text{ or } s) \tag{24}$$

and

$$T^j_N(t) := \int_{\hat{t}_N}^{t} ds\, I_j\, e^{-\frac{1}{\tau_j}(s-\hat{t}_N)}\, e^{\frac{1}{\tau_{Ca}}(s-t)}, \ (j = f \text{ or } s). \tag{25}$$

Furthermore, we define $S^j_{k+1,k}(t)$ as

$$\begin{aligned} S^j_{k+1,k}(t) :=& \int_{\hat{t}_k}^{\hat{t}_{k+1}} ds\, I_j\, e^{-\frac{1}{\tau_j}(s-\hat{t}_k)}\, e^{\frac{1}{\tau_{Ca}}(s-t)} \\ =& I_j \tau_{0j} e^{-\frac{1}{\tau_{Ca}}(t-\hat{t}_k)} \left[e^{\frac{1}{\tau_{0j}}(\hat{t}_{k+1}-\hat{t}_k)} - 1 \right], \end{aligned} \tag{26}$$

where τ_{0f} and τ_{0s} are defined as follows:

$$\frac{1}{\tau_{0j}} := \frac{1}{\tau_{Ca}} - \frac{1}{\tau_j}, \qquad (j = f \text{ or } s). \tag{27}$$

We write $t = \hat{t}_N + \epsilon \Delta t$, where $\epsilon \Delta t$ represents the time interval between the last spike time ($\hat{t}_N$) and the time to measure the calcium concentration (t). Substituting the formula into Eq. (26), we obtain

$$\begin{aligned} S^j_{k+1,k}(\hat{t}_N, \epsilon, \Delta t) :=& S^j_{k+1,k}(\hat{t}_N + \epsilon \Delta t) \\ =& I_j \tau_{0j} e^{-\frac{1}{\tau_{Ca}}(\epsilon \Delta t + \hat{t}_N - \hat{t}_k)} \left(e^{\frac{1}{\tau_{0j}} \delta_{k+1} \Delta t} - 1 \right). \end{aligned} \tag{28}$$

In the case of $0 \leq k \leq N-2$, we have

$$S^j_{k+1,k}(\hat{t}_N, \epsilon, \Delta t) = I_j \tau_{0j} e^{-\frac{1}{\tau_{Ca}} \epsilon \Delta t} \left(e^{-\frac{1}{\tau_j} \delta_{k+1} \Delta t} - e^{-\frac{1}{\tau_{Ca}} \delta_{k+1} \Delta t} \right) \prod_{k'=k+2}^{N} e^{-\frac{1}{\tau_{Ca}} \delta_{k'} \Delta t}. \tag{29}$$

In the case of $k = N-1$, we have

$$S^j_{N,N-1}(\hat{t}_N, \epsilon, \Delta t) = I_j \tau_{0j} e^{-\frac{1}{\tau_{Ca}} \epsilon \Delta t} \left(e^{-\frac{1}{\tau_j} \delta_N \Delta t} - e^{-\frac{1}{\tau_{Ca}} \delta_N \Delta t} \right). \tag{30}$$

Since we are interested in the long-term behavior of the calcium concentration and synaptic weights, but not in the fluctuations caused by each spike, we take the statistical average over one cycle. Let δ_k in Assumption 2 obey the probability density function $\rho(\delta)$. Then the statistical averages of $e^{-\frac{1}{\tau_{Ca}} \delta_k \Delta t}$ and $e^{-\frac{1}{\tau_j} \delta_k \Delta t}$ can be written as

$$\begin{aligned} r_{Ca} &:= \left\langle e^{-\frac{1}{\tau_{Ca}} \delta_k \Delta t} \right\rangle = \int_0^\infty \rho(\delta) e^{-\frac{1}{\tau_{Ca}} \delta \Delta t} d\delta, \\ r_j &:= \left\langle e^{-\frac{1}{\tau_j} \delta_k \Delta t} \right\rangle = \int_0^\infty \rho(\delta) e^{-\frac{1}{\tau_j} \delta \Delta t} d\delta. \end{aligned} \tag{31}$$

Hence, the statistical average of Eq. (29) is given as

$$\left\langle S^j_{k+1,k}(\hat{t}_N, \epsilon, \Delta t) \right\rangle = I_j \tau_{0j} e^{-\frac{1}{\tau_{Ca}} \epsilon \Delta t} (r_j - r_{Ca}) r_{Ca}^{N-k-1}. \tag{32}$$

Summing from $k = 0$ to $k = N-1$, the statistical average of Eq. (24) is obtained as

$$\left\langle S^j_{N-1}(\hat{t}_N, \epsilon, \Delta t)\right\rangle = I_j \tau_{0j} e^{-\frac{1}{\tau_{Ca}}\epsilon\Delta t}(r_j - r_{Ca})\frac{1 - r^N_{Ca}}{1 - r_{Ca}}. \tag{33}$$

In order to obtain the long-term behavior of $\left\langle S^j_{N-1}\right\rangle$, we take the limit $N \to \infty$. Since $r_{Ca} < 1$, and thus $r^N_{Ca} \to 0$ as $N \to \infty$, we obtain

$$\left\langle S^j_{N-1}(\epsilon, \Delta t)\right\rangle \simeq I_j \tau_{0j} \frac{r_j - r_{Ca}}{1 - r_{Ca}} \exp\left(-\frac{\epsilon\Delta t}{\tau_{Ca}}\right). \tag{34}$$

Similarly, using $t = \hat{t}_N + \epsilon\Delta t$ in Eq. (25) and taking the statistical average, we obtain (in the limit $N \to \infty$)

$$T^j_N(\epsilon, \Delta t) = I_j \tau_{0j}\left(e^{-\epsilon\Delta t/\tau_j} - e^{-\epsilon\Delta t/\tau_{Ca}}\right). \tag{35}$$

Using Eqs. (34) and (35), we obtain the statistical average of the postsynaptic calcium concentration as

$$\langle Ca(\Delta t, \epsilon)\rangle = H(V)\sum_{j=f,s} I_j \tau_{0j}\left[\exp\left(-\frac{\epsilon\Delta t}{\tau_j}\right) - \frac{1 - r_j}{1 - r_{Ca}}\exp\left(-\frac{\epsilon\Delta t}{\tau_{Ca}}\right)\right]. \tag{36}$$

Furthermore, the statistical average of this equation with respect to the observation time is given by

$$\langle Ca(\Delta t)\rangle = H(V)\sum_{j=f,s} I_j \tau_{0j}\left(r'_j - \frac{1 - r_j}{1 - r_{Ca}} r'_{Ca}\right), \tag{37}$$

where

$$r'_{Ca} := \left\langle e^{-\epsilon\Delta t/\tau_{Ca}}\right\rangle \quad \text{and} \quad r'_j := \left\langle e^{-\epsilon\Delta t/\tau_j}\right\rangle. \tag{38}$$

Calcium concentration of constant-ISI input. First, we calculate r_{Ca}, r_j, r'_{Ca}, and r'_j for the constant-ISI input, which are denoted as $r_{Ca;c}$, $r_{j;c}$, $r'_{Ca;c}$, and $r'_{j;c}$, respectively. In this case, the probability density function is given by $\rho_{Ca;c}(x) = \rho_{j;c}(x) = \delta(1 - x)$. Using this function in Eq. (31), we obtain

$$r_{Ca;c} = e^{-\frac{\Delta t}{\tau_{Ca}}}, \quad r_{j;c} = e^{-\frac{\Delta t}{\tau_j}}. \tag{39}$$

Since it is assumed that the sampling time follows a uniform distribution, r'_{Ca} and r'_j are expressed as follows:

$$r'_{Ca;c} = \frac{\tau_{Ca}}{\Delta t}\left(1 - e^{-\frac{\Delta t}{\tau_{Ca}}}\right), \quad r'_{j;c} = \frac{\tau_j}{\Delta t}\left(1 - e^{-\frac{\Delta t}{\tau_j}}\right). \tag{40}$$

Using Eqs. (39) and (40), we obtain the statistical average of the postsynaptic calcium concentration as a function of the spike interval Δt as follows:

$$\langle Ca(\Delta t)\rangle = H(V)\frac{\tau_{Ca}}{\Delta t}\sum_{j=f,s} I_j \tau_j\left[1 - \exp\left(-\frac{\Delta t}{\tau_j}\right)\right]. \tag{41}$$

Note that $H(V)$ is a slowly changing and monotonically increasing function of the membrane potential in the vicinity of the resting membrane potential (− 65 mV), and the duration of depolarization by EPSP is approximately 50 to 100 ms at most. Therefore, the increase in the average membrane potential remains at approximately 5.4 mV, even in the case of the highest frequency, e.g., 100 Hz. The average membrane potential, moreover, increases linearly with the stimulation frequency. Thus, $H(V(\Delta t))$ is approximately expressed as a quadric function of $1/\Delta t (= f)$. With this approximation, we obtain the following expression:

$$\begin{aligned}\left\langle Ca_c(f)\right\rangle = {} & \tau_{Ca} f(\gamma_0 + \gamma_1 f + \gamma_2 f^2) \\ & \times \sum_{j=f,s} I_j \tau_j\left[1 - \exp\left(-\frac{1}{\tau_j \cdot f}\right)\right].\end{aligned} \tag{42}$$

Here, $\gamma_0 = 1.28 \times 10^{-2}$ mV, $\gamma_1 = 3.20 \times 10^{-2}$ mV ms, and $\gamma_2 = 3.71 \times 10^{-2}$ mV m^2. These values are determined by finding the relation between the input frequency and the time average of $V(t)$ in Eq. (16) and by substituting the obtained values into the quadratic approximation of $H(V)$.

Calcium concentration of Poisson input. The time interval of the spike sequence according to the Poisson process follows an exponential distribution, the probability density function of which is given by $\rho_{Ca;poi}(x) = \rho_{j;poi}(x) = e^{-x}$. Then, we can calculate r_{Ca} and r_j for the Poisson input as

$$r_{Ca;poi} = \frac{\tau_{Ca}}{\tau_{Ca} + \Delta t}, \quad r_{j;poi} = \frac{\tau_j}{\tau_j + \Delta t}. \tag{43}$$

Since the spike interval fluctuates stochastically in the Poisson input, the observation time is considered to fluctuate with the same statistics. Then, r'_{Ca} and r'_j in the Poisson input, written as $r'_{Ca;poi}$ and $r'_{j;poi}$, are equal to $r_{Ca;poi}$ and $r_{j;poi}$, respectively. Substituting $r_{Ca;poi}$, $r_{j;poi}$, $r'_{Ca;poi}$, and $r'_{j;poi}$, we obtain the statistical average of the postsynaptic calcium concentration receiving Poisson input as a function of the average frequency as follows:

$$\left\langle Ca_{poi}(f)\right\rangle = \tau_{Ca} f(\gamma_0 + \gamma_1 f + \gamma_2 f^2) \sum_{j=f,s} I_j \frac{\tau_j}{\tau_j f + 1}. \tag{44}$$

Calcium concentration of gamma process input. The time interval of the spike sequence according to the gamma process follows a gamma distribution, the general formula for the probability density function of which is given as

$$\rho_{Ca;\Gamma}(x;\alpha) = \rho_{j;\Gamma}(x;\alpha) = \frac{1}{\Gamma(\alpha)} x^{\alpha-1} e^{-x}, \tag{45}$$

where α is the shape parameter, and Γ is the gamma function, which is given by

$$\Gamma(\alpha) := \int_0^\infty t^{\alpha-1} e^{-t} dt. \tag{46}$$

Since, as in the Poisson input, the spike interval and the sampling time fluctuate with the same statistics, $r_{Ca} = r'_{Ca} =: r_{Ca:\Gamma}$ and $r_j = r'_j =: r_{j:\Gamma}$ in Eq. (36). Thus, we obtain

$$r_{Ca:\Gamma} = \left(\frac{\tau_{Ca}}{\tau_{Ca} + \Delta t}\right)^\alpha, \quad r_{j:\Gamma} = \left(\frac{\tau_j}{\tau_j + \Delta t}\right)^\alpha. \tag{47}$$

Noting that the average spike interval of the gamma distribution input is $\alpha \Delta t$, we can express the statistical average of the postsynaptic calcium concentration with gamma process input as follows:

$$\begin{aligned}\left\langle Ca_\Gamma(f)\right\rangle = {} & (\gamma_0 + \gamma_1 f + \gamma_2 f^2)(\alpha f)^\alpha \\ & \times \sum_{j=f,s} I_j \tau_{0j} \left[\frac{\left(\frac{\tau_j}{\alpha\tau_j f+1}\right)^\alpha - \left(\frac{\tau_{Ca}}{\alpha\tau_{Ca} f+1}\right)^\alpha}{1 - \left(\frac{\alpha\tau_{Ca} f}{\alpha\tau_{Ca} f+1}\right)^\alpha}\right].\end{aligned} \tag{48}$$

Derivation of the approximate analytic solutions for the synaptic weight as functions of the average frequency of constant-ISI, Poisson, and gamma process inputs. According to the calcium control hypothesis reported by Shouval et al., the time derivative of the synaptic efficacy W is expressed as a function of intracellular calcium concentration as indicated in Eqs. (9)–(11)[33]. Equation (9) indicates that the synaptic strength approaches an asymptotic value $\Omega(Ca(t))$ with time constant $1/\eta(Ca(t))$. The functional form of $\Omega(Ca(t))$ in Eq. (11) is based qualitatively on the notion that a moderate rise in calcium leads to a decrease in the synaptic weight, whereas a large rise leads to an increase in the synaptic weight. This notion is closely related to the BCM theory, which states that weak synaptic input activity results in a decrease in synaptic strength, whereas strong input leads to an increase in synaptic weight[4,78].

Although it is difficult to find the exact relation between the synaptic weight W and the stimulation rate f analytically, we can obtain an approximate relation by assuming that $W(t)$ converges to a stationary solution in the macroscopic time scale, i.e.,

$$\lim_{t\to\infty} W(t,f) := \left\langle W(f)\right\rangle \approx \left\langle \Omega(Ca(f))\right\rangle. \tag{49}$$

In order to calculate $\left\langle \Omega(Ca(f))\right\rangle$, we express the postsynaptic calcium concentration as

$$\begin{aligned} Ca(\Delta t, x, \epsilon | r_{Ca}, r_j) &\approx \lim_{N\to\infty} H(V) \sum_{j=f,s} \left[T^j + S^j_{N,N-1} + \sum_{k=0}^{N-2} S^j_{k+1,k}\right] \\ &= H(V) \sum_{j=f,s} I_j \tau_{0j} \left[e^{-\frac{1}{\tau_j}\epsilon\Delta t} - e^{-\frac{1}{\tau_{Ca}}\epsilon\Delta t}\right. \\ &\quad + e^{-\frac{1}{\tau_{Ca}}\epsilon\Delta t}\left(e^{-\frac{1}{\tau_j}x\Delta t} - e^{-\frac{1}{\tau_{Ca}}x\Delta t}\right) \\ &\quad \left. + e^{-\frac{1}{\tau_{Ca}}(x+\epsilon)\Delta t}\left(\frac{r_j - r_{Ca}}{1 - r_{Ca}}\right)\right], \end{aligned} \tag{50}$$

where $x = \delta_N, r_{Ca}$, and r_j are defined in Eq. (31). By substituting Eq. (50) into the expression for $\Omega(Ca)$ in Eq. (11) and calculating the statistical average with respect to x and ϵ, we obtain an approximate analytical solution for the synaptic weight as a function of the average input frequency.

In the case of the constant-ISI input, the time interval of the spike sequence obeys the probability density function $\rho(x) = \delta(1 - x)$. Moreover, the time interval from the last spike to the sampling time obeys a uniform

distribution. Thus, we obtain the statistical average of the synaptic weight as a function of input frequency f as follows:

$$\langle W_c(f)\rangle = \int_0^\infty dx \int_0^1 d\epsilon\ \delta(1-x)\Omega(Ca(1/f,x,\epsilon|r_{Ca;c},r_{j;c})). \tag{51}$$

In the cases of the Poisson input and gamma process input, the spike interval as well as the time interval between the last spike and the observation time obey exponential and gamma distributions, respectively. Thus, the statistical average of the synaptic weight as a function of input frequency f in these inputs are calculated as follows:

$$\begin{aligned}\langle W_{poi}(f)\rangle = &\int_0^\infty dx \int_0^\infty d\epsilon\ e^{-(x+\epsilon)} \\ &\times\ \Omega(Ca(1/f,x,\epsilon|r_{Ca;poi},r_{j;poi})),\end{aligned} \tag{52}$$

$$\begin{aligned}\langle W_\Gamma(f)\rangle = &\frac{1}{\Gamma(\alpha)^2}\int_0^\infty dx \int_0^\infty d\epsilon\ (x\epsilon)^{\alpha-1}e^{-(x+\epsilon)} \\ &\times\ \Omega(Ca(1/\alpha f,x,\epsilon|r_{Ca;\Gamma},r_{j;\Gamma})).\end{aligned} \tag{53}$$

Received: 22 February 2020; Accepted: 4 August 2020
Published online: 18 August 2020

References

1. Martin, S. J., Grimwood, P. D. & Morris, R. G. Synaptic plasticity and memory: an evaluation of the hypothesis. *Annu. Rev. Neurosci.* **23**, 649–711. https://doi.org/10.1146/annurev.neuro.23.1.649 (2000).
2. Sjostrom, P. J., Turrigiano, G. G. & Nelson, S. B. Rate, timing, and cooperativity jointly determine cortical synaptic plasticity. *Neuron* **32**, 1149–64 (2001).
3. Weissenberger, F., Gauy, M. M., Lengler, J., Meier, F. & Steger, A. Voltage dependence of synaptic plasticity is essential for rate based learning with short stimuli. *Sci. Rep.* **8**, 4609. https://doi.org/10.1038/s41598-018-22781-0 (2018).
4. Bienenstock, E. L., Cooper, L. N. & Munro, P. W. Theory for the development of neuron selectivity: orientation specificity and binocular interaction in visual cortex. *J. Neurosci.* **2**, 32–48 (1982).
5. Bliss, T. V. & Lomo, T. Long-lasting potentiation of synaptic transmission in the dentate area of the anaesthetized rabbit following stimulation of the perforant path. *J. Physiol.* **232**, 331–56 (1973).
6. Bliss, T. V. & Gardner-Medwin, A. R. Long-lasting potentiation of synaptic transmission in the dentate area of the unanaestetized rabbit following stimulation of the perforant path. *J. Physiol.* **232**, 357–74 (1973).
7. Bliss, T. V. & Collingridge, G. L. A synaptic model of memory: long-term potentiation in the hippocampus. *Nature* **361**, 31–9. https://doi.org/10.1038/361031a0 (1993).
8. Kirkwood, A., Dudek, S. M., Gold, J. T., Aizenman, C. D. & Bear, M. F. Common forms of synaptic plasticity in the hippocampus and neocortex in vitro. *Science* **260**, 1518–21 (1993).
9. Dudek, S. M. & Bear, M. F. Homosynaptic long-term depression in area CA1 of hippocampus and effects of N-methyl-D-aspartate receptor blockade. *Proc. Natl. Acad. Sci. USA* **89**, 4363–7 (1992).
10. Mulkey, R. M. & Malenka, R. C. Mechanisms underlying induction of homosynaptic long-term depression in area CA1 of the hippocampus. *Neuron* **9**, 967–75 (1992).
11. Artola, A. & Singer, W. Long-term depression of excitatory synaptic transmission and its relationship to long-term potentiation. *Trends Neurosci.* **16**, 480–7 (1993).
12. Gerstner, W. & Kistler, W. M. *Spiking Neuron Models : Single Neurons, Populations, Plasticity* (Cambridge University Press, Cambridge, 2002).
13. Song, S., Miller, K. D. & Abbott, L. F. Competitive hebbian learning through spike-timing-dependent synaptic plasticity. *Nat. Neurosci.* **3**, 919–26. https://doi.org/10.1038/78829 (2000).
14. Bi, G. Q. & Poo, M. M. Synaptic modifications in cultured hippocampal neurons: Dependence on spike timing, synaptic strength, and postsynaptic cell type. *J. Neurosci.* **18**, 10464–72 (1998).
15. Gerstner, W., Kempter, R., van Hemmen, J. L. & Wagner, H. A neuronal learning rule for sub-millisecond temporal coding. *Nature* **383**, 76–81. https://doi.org/10.1038/383076a0 (1996).
16. Markram, H., Lubke, J., Frotscher, M. & Sakmann, B. Regulation of synaptic efficacy by coincidence of postsynaptic APs and EPSPs. *Science* **275**, 213–5 (1997).
17. Debanne, D., Gahwiler, B. H. & Thompson, S. M. Long-term synaptic plasticity between pairs of individual CA3 pyramidal cells in rat hippocampal slice cultures. *J. Physiol.* **507**(Pt 1), 237–47 (1998).
18. Feldman, D. E. Timing-based LTP and LTD at vertical inputs to layer II/III pyramidal cells in rat barrel cortex. *Neuron* **27**, 45–56 (2000).
19. Zhang, L. I., Tao, H. W., Holt, C. E., Harris, W. A. & Poo, M. A critical window for cooperation and competition among developing retinotectal synapses. *Nature* **395**, 37–44. https://doi.org/10.1038/25665 (1998).
20. Graupner, M., Wallisch, P. & Ostojic, S. Natural firing patterns imply low sensitivity of synaptic plasticity to spike timing compared with firing rate. *J. Neurosci.* **36**, 11238–11258. https://doi.org/10.1523/JNEUROSCI.0104-16.2016 (2016).
21. Softky, W. R. & Koch, C. The highly irregular firing of cortical cells is inconsistent with temporal integration of random EPSPs. *J. Neurosci.* **13**, 334–50 (1993).
22. Knierim, J. J. & van Essen, D. C. Neuronal responses to static texture patterns in area v1 of the alert macaque monkey. *J. Neurophysiol.* **67**, 961–80. https://doi.org/10.1152/jn.1992.67.4.961 (1992).
23. Chance, F. & Abbott, L. F. *Simulating in Vivo Background Activity in a Slice With The Dynamic Clamp* 73–87 (Springer, Berlin, 2009).
24. Jacobson, G. A. *et al.* Subthreshold voltage noise of rat neocortical pyramidal neurones. *J. Physiol.* **564**, 145–60. https://doi.org/10.1113/jphysiol.2004.080903 (2005).
25. London, M., Roth, A., Beeren, L., Hausser, M. & Latham, P. E. Sensitivity to perturbations in vivo implies high noise and suggests rate coding in cortex. *Nature* **466**, 123–7. https://doi.org/10.1146/annurev.neuro.23.1.6490 (2010).

26. Madadi Asl, M., Valizadeh, A. & Tass, P. A. Dendritic and axonal propagation delays determine emergent structures of neuronal networks with plastic synapses. *Sci. Rep.* **7**, 39682. https://doi.org/10.1146/annurev.neuro.23.1.6491 (2017).
27. Madadi Asl, M., Valizadeh, A. & Tass, P. A. Delay-induced multistability and loop formation in neuronal networks with spike-timing-dependent plasticity. *Sci. Rep.* **8**, 12068. https://doi.org/10.1146/annurev.neuro.23.1.6492 (2018).
28. Li, M. & Tsien, J. Z. Neural code-neural self-information theory on how cell-assembly code rises from spike time and neuronal variability. *Front. Cell Neurosci.* **11**, 236. https://doi.org/10.1146/annurev.neuro.23.1.6493 (2017).
29. Graupner, M. & Brunel, N. Calcium-based plasticity model explains sensitivity of synaptic changes to spike pattern, rate, and dendritic location. *Proc. Natl. Acad. Sci. USA* **109**, 3991–6. https://doi.org/10.1146/annurev.neuro.23.1.6494 (2012).
30. Sjostrom, P. J. & Hausser, M. A cooperative switch determines the sign of synaptic plasticity in distal dendrites of neocortical pyramidal neurons. *Neuron* **51**, 227–38. https://doi.org/10.1146/annurev.neuro.23.1.6495 (2006).
31. Nobukawa, S. & Nishimura, H. Enhancement of spike-timing-dependent plasticity in spiking neural systems with noise. *Int. J. Neural Syst.* **26**, 1550040. https://doi.org/10.1146/annurev.neuro.23.1.6496 (2016).
32. Yasuda, H. *et al.* Novel class of neural stochastic resonance and error-free information transfer. *Phys. Rev. Lett.* **100**, 118103. https://doi.org/10.1146/annurev.neuro.23.1.6497 (2008).
33. Shouval, H. Z., Bear, M. F. & Cooper, L. N. A unified model of nmda receptor-dependent bidirectional synaptic plasticity. *Proc. Natl. Acad. Sci. USA* **99**, 10831–6. https://doi.org/10.1146/annurev.neuro.23.1.6498 (2002).
34. Cummings, J. A., Mulkey, R. M., Nicoll, R. A. & Malenka, R. C. Ca^{2+} signaling requirements for long-term depression in the hippocampus. *Neuron* **16**, 825–33 (1996).
35. Cormier, R. J., Greenwood, A. C. & Connor, J. A. Bidirectional synaptic plasticity correlated with the magnitude of dendritic calcium transients above a threshold. *J. Neurophysiol.* **85**, 399–406. https://doi.org/10.1146/annurev.neuro.23.1.6499 (2001).
36. Cho, K., Aggleton, J. P., Brown, M. W. & Bashir, Z. I. An experimental test of the role of postsynaptic calcium levels in determining synaptic strength using perirhinal cortex of rat. *J. Physiol.* **532**, 459–66 (2001).
37. Yang, S. N., Tang, Y. G. & Zucker, R. S. Selective induction of LTP and LTD by postsynaptic $[Ca^{2+}]$i elevation. *J. Neurophysiol.* **81**, 781–7. https://doi.org/10.1038/s41598-018-22781-00 (1999).
38. Jones, R. S. & Woodhall, G. L. Background synaptic activity in rat entorhinal cortical neurones: Differential control of transmitter release by presynaptic receptors. *J. Physiol.* **562**, 107–20. https://doi.org/10.1038/s41598-018-22781-01 (2005).
39. Rapp, M., Yarom, Y. & Segev, I. Modeling back propagating action potential in weakly excitable dendrites of neocortical pyramidal cells. *Proc. Natl. Acad. Sci. USA* **93**, 11985–90 (1996).
40. Bereshpolova, Y., Amitai, Y., Gusev, A. G., Stoelzel, C. R. & Swadlow, H. A. Dendritic backpropagation and the state of the awake neocortex. *J. Neurosci.* **27**, 9392–9. https://doi.org/10.1038/s41598-018-22781-02 (2007).
41. Faisal, A. A., Selen, L. P. & Wolpert, D. M. Noise in the nervous system. *Nat. Rev. Neurosci.* **9**, 292–303. https://doi.org/10.1038/s41598-018-22781-03 (2008).
42. Ahmed, B., Anderson, J. C., Douglas, R. J., Martin, K. A. & Whitteridge, D. Estimates of the net excitatory currents evoked by visual stimulation of identified neurons in cat visual cortex. *Cereb. Cortex* **8**, 462–76 (1998).
43. Liu, Y. H. & Wang, X. J. Spike-frequency adaptation of a generalized leaky integrate-and-fire model neuron. *J. Comput. Neurosci.* **10**, 25–45 (2001).
44. Shouval, H. Z. & Kalantzis, G. Stochastic properties of synaptic transmission affect the shape of spike time-dependent plasticity curves. *J. Neurophysiol.* **93**, 1069–73. https://doi.org/10.1038/s41598-018-22781-04 (2005).
45. Bush, D. & Jin, Y. Calcium control of triphasic hippocampal STDP. *J. Comput. Neurosci.* **33**, 495–514. https://doi.org/10.1038/s41598-018-22781-05 (2012).
46. Yeung, L. C., Castellani, G. C. & Shouval, H. Z. Analysis of the intraspinal calcium dynamics and its implications for the plasticity of spiking neurons. *Phys. Rev. E Stat. Nonlinear Soft Matter Phys.* **69**, 011907. https://doi.org/10.1038/s41598-018-22781-06 (2004).
47. Speed, H. E. & Dobrunz, L. E. Developmental decrease in short-term facilitation at schaffer collateral synapses in hippocampus is mGluR1 sensitive. *J. Neurophysiol.* **99**, 799–813. https://doi.org/10.1038/s41598-018-22781-07 (2008).
48. Brunel, N. Dynamics of sparsely connected networks of excitatory and inhibitory spiking neurons. *J. Comput. Neurosci.* **8**, 183–208 (2000).
49. Deger, M., Helias, M., Boucsein, C. & Rotter, S. Statistical properties of superimposed stationary spike trains. *J. Comput. Neurosci.* **32**, 443–63. https://doi.org/10.1038/s41598-018-22781-08 (2012).
50. Maimon, G. & Assad, J. A. Beyond poisson: Increased spike-time regularity across primate parietal cortex. *Neuron* **62**, 426–40. https://doi.org/10.1038/s41598-018-22781-09 (2009).
51. Baker, S. N. & Lemon, R. N. Precise spatiotemporal repeating patterns in monkey primary and supplementary motor areas occur at chance levels. *J. Neurophysiol.* **84**, 1770–80 (2000).
52. Burton, S. D. & Urban, N. N. Rapid feedforward inhibition and asynchronous excitation regulate granule cell activity in the mammalian main olfactory bulb. *J. Neurosci.* **35**, 14103–22. https://doi.org/10.1038/361031a00 (2015).
53. Li, M. *et al.* Spike-timing pattern operates as gamma-distribution across cell types, regions and animal species and is essential for naturally-occurring cognitive states. Biorxiv 145813 (2018).
54. Moore, J. J. *et al.* Dynamics of cortical dendritic membrane potential and spikes in freely behaving rats. *Science*https://doi.org/10.1126/science.aaj1497 *(2017).*
55. Gjorgjieva, J., Clopath, C., Audet, J. & Pfister, J. P. A triplet spike-timing-dependent plasticity model generalizes the Bienenstock–Cooper–Munro rule to higher-order spatiotemporal correlations. *Proc. Natl. Acad. Sci. USA* **108**, 19383–8. https://doi.org/10.1073/pnas.1105933108 (2011).
56. Pfister, J. P. & Gerstner, W. Triplets of spikes in a model of spike timing-dependent plasticity. *J. Neurosci.* **26**, 9673–82. https://doi.org/10.1523/JNEUROSCI.1425-06.2006 (2006).
57. Carrillo-Medina, J. L. & Latorre, R. Implementing signature neural networks with spiking neurons. *Front. Comput. Neurosci.* **10**, 132. https://doi.org/10.3389/fncom.2016.00132 (2016).
58. Bialek, W., Rieke, F., de Ruyter van Steveninck, R. R. & Warland, D. Reading a neural code. *Science* **252**, 1854–7 (1991).
59. Kandel, E. R. *et al.* (eds) *Principles of Neural Science* 5th edn. (Elsevier Science Publishing Co., Inc., New York, 2013).
60. Rao, R. P. N., Olshausen, B. A. & Lewicki, M. S. Probabilistic models of the brain: Perception and neural function. In *Neural Information Processing Series* (eds Rao, R. P. N. *et al.*) (MIT Press, Cambridge, 2002).
61. Zhao, C. *et al.* Spike-time-dependent encoding for neuromorphic processors. *J. Emerg. Technol. Comput. Syst.* **12**, 1–21. https://doi.org/10.1145/2738040 (2015).
62. Panzeri, S., Brunel, N., Logothetis, N. K. & Kayser, C. Sensory neural codes using multiplexed temporal scales. *Trends Neurosci.* **33**, 111–20. https://doi.org/10.1016/j.tins.2009.12.001 (2010).
63. Latorre, R., Rodriguez, F. B. & Varona, P. Neural signatures: Multiple coding in spiking-bursting cells. *Biol. Cybern.* **95**, 169–83. https://doi.org/10.1007/s00422-006-0077-5 (2006).
64. Kayser, C., Montemurro, M. A., Logothetis, N. K. & Panzeri, S. Spike-phase coding boosts and stabilizes information carried by spatial and temporal spike patterns. *Neuron* **61**, 597–608. https://doi.org/10.1016/j.neuron.2009.01.008 (2009).
65. Hu, E. *et al.* A glutamatergic spine model to enable multi-scale modeling of nonlinear calcium dynamics. *Front. Comput. Neurosci.* **12**, 58. https://doi.org/10.3389/fncom.2018.00058 (2018).
66. Minelli, A. *et al.* Cellular and subcellular localization of Na^{+}–Ca^{2+} exchanger protein isoforms, NCX1, NCX2, and NCX3 in cerebral cortex and hippocampus of adult rat. *Cell Calcium* **41**, 221–34. https://doi.org/10.1016/j.ceca.2006.06.004 (2007).

67. Jeon, D. *et al.* Enhanced learning and memory in mice lacking Na^+/Ca^{2+} exchanger 2. *Neuron* **38**, 965–76 (2003).
68. Secondo, A. *et al.* Involvement of the Na^+/Ca^{2+} exchanger isoform 1 (NCX1) in neuronal growth factor (NGF)-induced neuronal differentiation through Ca^{2+}-dependent AKT phosphorylation. *J. Biol. Chem.* **290**, 1319–31. https://doi.org/10.1074/jbc.M114.555516 (2015).
69. Moriguchi, S. *et al.* Reduced expression of Na^+/Ca^{2+} exchangers is associated with cognitive deficits seen in Alzheimer's disease model mice. *Neuropharmacology* **131**, 291–303. https://doi.org/10.1016/j.neuropharm.2017.12.037 (2018).
70. Asano, S. *et al.* Nitroprusside and cyclic GMP stimulate Na^+-Ca^{2+} exchange activity in neuronal preparations and cultured rat astrocytes. *J. Neurochem.* **64**, 2437–41 (1995).
71. Destexhe, A., Rudolph, M. & Pare, D. The high-conductance state of neocortical neurons in vivo. *Nat. Rev. Neurosci.* **4**, 739–51. https://doi.org/10.1038/nrn1198 (2003).
72. Stacey, W. C. & Durand, D. M. Synaptic noise improves detection of subthreshold signals in hippocampal CA1 neurons. *J. Neurophysiol.* **86**, 1104–12. https://doi.org/10.1152/jn.2001.86.3.1104 (2001).
73. Remy, S. & Spruston, N. Dendritic spikes induce single-burst long-term potentiation. *Proc. Natl. Acad. Sci. USA* **104**, 17192–7. https://doi.org/10.1073/pnas.0707919104 (2007).
74. Costa, R. P., Froemke, R. C., Sjostrom, P. J. & van Rossum, M. C. Unified pre- and postsynaptic long-term plasticity enables reliable and flexible learning. *Elife*https://doi.org/10.7554/eLife.09457 *(2015).*
75. Stuart, G. J. & Hausser, M. Dendritic coincidence detection of EPSPs and action potentials. *Nat. Neurosci.* **4**, 63–71. https://doi.org/10.1038/82910 (2001).
76. Zheng, Y. & Schwabe, L. Shaping synaptic learning by the duration of postsynaptic action potential in a new STDP model. *PLoS ONE* **9**, e88592. https://doi.org/10.1371/journal.pone.0088592 (2014).
77. Yaron-Jakoubovitch, A., Jacobson, G. A., Koch, C., Segev, I. & Yarom, Y. A paradoxical isopotentiality: A spatially uniform noise spectrum in neocortical pyramidal cells. *Front. Cell Neurosci.* **2**, 3. https://doi.org/10.3389/neuro.03.003.2008 (2008).
78. Izhikevich, E. M. & Desai, N. S. Relating stdp to bcm. *Neural Comput.* **15**, 1511–23. https://doi.org/10.1162/089976603321891783 (2003).

Acknowledgements

This work was supported by JSPS KAKENHI Grant Numbers JP18K10858, JP18K10999.

Author contributions

K.H. conceived of the presented idea. K.H. developed the theory. K.H. and O.A. designed the model and the computational framework. K.H. and T.N. performed the analytical calculation. K.H. and O.Y. performed the numerical simulation. K.H., T.K., Y.Y., S.I. and T.N. analysed the data. All authors reviewed the manuscript.

Competing interests

The authors declare no competing interests.

Additional information

Supplementary information is available for this paper at https://doi.org/10.1038/s41598-020-70876-4.

Correspondence and requests for materials should be addressed to K.H.

Reprints and permissions information is available at www.nature.com/reprints.

Publisher's note Springer Nature remains neutral with regard to jurisdictional claims in published maps and institutional affiliations.